Main Manuscript for

A hepatocyte-specific transcriptional program driven by Rela and Stat3 exacerbates experimental colitis in mice by modulating bile synthesis

Jyotsna [1], Binayak Sarkar [1], Mohit Yadav [1], Alvina Deka [2], Manasvini Markandey [5], Priyadarshini Sanyal [3], Perumal Nagarajan [1], Nilesh Gaikward [4], Vineet Ahuja [5], Debasisa Mohanty [1], Soumen Basak [2], Rajesh S Gokhale [1,6]

Affiliation: 1. Immunometabolism Laboratory, National Institute of Immunology, New Delhi 110067;

2. System Immunology Laboratory, National Institute of Immunology, New Delhi 110067;

3. Center for Cellular and Molecular Biology, Hyderabad 500007, Telangana;

4. Gaikwad Steroidomics Lab LLC, Davis, CA 95616;

5. Department of GastroEnterology, All India Institute of Medical Sciences, New Delhi 110067;

6. Department of Biology, Indian Institute of Science Education and Research, Pashan, Pune 411008, Maharashtra;

Corresponding author: Rajesh S. Gokhale.

Email: rsg.nii.ac.in

Author Contributions: J and RSG conceptualized the project. J, BS, MY, AD, MM developed the methodology. J and BS conducted the formal analysis. J, BS, MY, AD, MM, PS performed the investigation. DM, SB, RSG acquired resources for the study. J, SB, RSG wrote the original draft of the manuscript. J, VA, DM, SB, RSG reviewed and edited the manuscript. J was responsible for visualization. RSG supervised the project.

Competing Interest Statement: The authors declare no competing interest.

Keywords: Rela, Stat3, bile acid, colitis, inflammation.

This PDF file includes:

Main Text
Figures 1 to 6 and S1 to S5
Tables S1 to S7

Abstract

Hepatic factors secreted by the liver promote homeostasis and are pivotal to maintain liver-gut axis. Dysfunctional interactions between the liver and the intestine stimulate varied pathological outcomes through its bidirectional portal communication for example an aberrant bile acid metabolism has been reported in inflammatory bowel disease (IBD). However, the molecular mechanisms underlying these crosstalks that perpetuate intestinal permeability and inflammation remains obscure. Here, we identify a novel hepatic gene program regulated by Rela and Stat3 that accentuates the inflammation in an acute experimental colitis model. Hepatocyte specific ablation of Rela and Stat3 reduces the levels of primary bile acids in both liver and gut and shows restricted colitogenic phenotype. On supplementation of chenodeoxycholic acid (CDCA), knock-out mice show enhanced colitis-induced alterations. This study provides persuasive evidence for the development of multi-organ strategies for treating IBD and identifies a hepatocyte-specific *rela-stat3* network as a promising therapeutic target.

Main Text

Introduction

Under physiological conditions, the liver is continuously exposed to gut derived antigens which are either food derived or a product of microbial metabolism [1]. The continuous interaction of extraneous antigen with the liver tissue makes it an tolerogenic organ and in turn, justifies its unique anatomical location [2]. However, during inflammation/dysbiosis, like in the case of inflammatory bowel disease (IBD), there is an unregulated exchange of molecules across the gut vascular barrier, which potentially rewires the immunological as well as metabolic milieu [3,4]. In the past decade several have focused on dissecting alterations in this crosstalk as it is thought the mechanistic understanding will pave the way towards effective multi-organ interventions [5,6].

Clinically, IBD overlaps with hepatobiliary conditions, as 30% IBD cases have abnormal liver tests and around 5% of them develop chronic hepatobiliary disease [7, 8]. The first responders to extraneous dangers due to leakiness of the gut during colitis are the Kupffer cells, which keep a check on the content flowing through the portal system [9]. The Kupffer cells have shown to switch from a pro to anti-inflammatory state in response to signals received during colitis [10]. However, these are not the only cells that are reprogrammed during the course of colitis development. Liver hepatocytes that are known to secrete a variety of factors, including complement proteins, hepatokines, bile acids etc. have also been shown to have an altered metabolic state [11, 12]. Among the secreted factors, albumin is the most abundantly produced

serum protein, which is implicated in the maintenance of redox balance and attenuates DSS induced colitis [13]. Several other proteins like FNDC4 that is predominantly produced by the liver and are implicated in attenuating colonic inflammation, emphasizing the importance of the liver secretome [14]. Similarly, bile acids are also known to play a pivotal role in regulating mucosal immune responses. Primary bile acids produced by the liver are often related to an enhanced proinflammatory state and its turnover to secondary bile acids is considered to be a critical step in the maintenance of homeostasis [15]. The primary bile acids have been reported to accumulate in the inflamed colon, this suggesting some intriguing crosstalk between the gut and liver [16]. However, how the liver perceives signals due to the disease mediated impaired gut barrier to rewire secretory machinery and tackle the enhanced endotoxins influx.

Through this study, we propose Rela and Stat3 as key responders of inflammatory signaling in the liver tissue in response to intestinal aberration. We further define a colitis resistance model based on the liver specific knockout animals and propose a Rela/Stat3-CYP enzyme mediated elevation of primary bile acid. Our study revealed an immune-mediated damage to the gut driven by a primary BA (bile acid), chenodeoxycholic acid. Our study establishes not only the functional significance of hepatic Rela and Stat3 in intestinal inflammation but also underscores the therapeutic opportunities of targeting multiorgan crosstalk in inflammatory diseases.

Results

Engagement of hepatic Rela and/or Stat3 pathways in murine colitis model

Several studies have shown that the gut-liver bidirectional communication is critical in both the establishment and progression of IBD. Towards identifying liver pathways that affect intestinal impairment during IBD, we firstly examined whether 2% dextran sodium sulphate (DSS)-induced acute experimental colitis results in changes in liver pathophysiology. Analysis of biochemical parameters on day 6 of DSS treatment showed no significant alterations in the levels of alanine aminotransferase (ALT), aspartate aminotransferase (AST), gamma-glutamyl transferase (GGT) and bilirubin (Figure S1a). Further, histological studies of these treated liver tissues from C57BL/6 mice showed neither morphological differences nor any hepatocellular fibrosis (Figure S1b). Thus, in general the liver functionalities are maintained and no major damage in the liver tissue occurs in the colitogenic mice model. We then performed global transcriptomic studies of the liver tissue from day 6 colitogenic mice. Unsupervised clustering of the transcriptome data by principal component analysis (PCA) segregated the treated and control samples on PC1 with a variance of 53% (Figure S1c). Immunological and metabolic pathways

appeared to be enriched in the list of regulated pathways. LPS mediated signaling in the liver was identified as amongst the key differentially expressed systems (Figure 1A). It is proposed that microbial components, including LPS from the gut, can reach the liver through portal blood, activating the hepatic immune response during colitis-mediated barrier impairment. Interestingly, Rela and Stat3 are two important transcription factors activated by the microbial LPS and these two pathways frequently converge to elicit protective responses [17, 18, 19, 20]. Further analysis of transcript abundance of Rela, Stat3, and other downstream genes reflected higher transcript abundance in the DSS treated group as compared to the control (Figure 1B). Functional activation of Rela and Stat3 pathways requires phosphorylation of key residues, which we investigated in the liver sections of DSS treated mice. Immunostaining studies showed an enhanced signal intensity of p-Rela (Ser536), p-Stat3 (Ser727) and p-Stat3 (Tyr705) in the treated liver sections, as compared to untreated samples (Figure 1C).

We then examined time-dependent phosphorylation status of the two proteins of the liver post 0, 2, 4, and 6 days of DSS treatment. The RelA phosphorylation at Ser536 peaks at day 2 (about eight fold increase) following which a two to three fold increase was sustained till day 6 (Figure 1D and E). The Stat3 phosphorylation at Ser727 increases gradually from day 2 (eight-fold) to day 6 (seventeen-fold). Tyrosine phosphorylation on the other hand, is transient and can be detected at day 4 (nine-fold) post treatment (Figure 1D and E). Together, this analysis establishes that RelA and Stat3 factors are activated in the liver and we hypothesize that this transcriptional network could play a key role in balancing the liver - gut crosstalk.

Hepatocyte-specific functions of Rela and Stat3 exacerbate experimental colitis

In order to discern the importance of transcriptional networks regulated by Rela and Stat3 we utilized a hepatocyte specific knockout model. The Cre recombinase under albumin promoter drives the deletion of Rela and/or Stat3 in a tissue specific manner (Figure S2a and S2b). To address the question, if ablation of Rela and Stat3 functioning in hepatocytes could modulate colonic inflammation, we subjected $rela^{\Delta hep}$, $stat3^{\Delta hep}$, $rela^{\Delta hep}stat3^{\Delta hep}$ and wildtype littermates mice to acute DSS treatment. Previous studies suggest development of colitis in acute models is accompanied by shortening of the colon length, diarrhea and rectal bleeding which is measured as the disease activity index (DAI) [21]. Time course measurement of DAI in the wild type showed expected increase from day three (Figure 2A). While the DAI in $rela^{\Delta hep}$ mice was parallel to that observed in wildtype mice, $stat3^{\Delta hep}$ mice displayed a subtle decrease in the DAI score, particularly on day five. Surprisingly, $rela^{\Delta hep}stat3^{\Delta hep}$ mice were almost resistant to induction of colitis, and only a minor increase in the DAI could be seen on day 6 post-onset of DSS treatment (Figure 2A). Concurrently, DSS treatment for six days showed substantial shortening of the colon

length in wildtype, *rela*$^{\Delta hep}$, and *stat3*$^{\Delta hep}$ mice, but not in *rela*$^{\Delta hep}$*stat3*$^{\Delta hep}$ mice (Figure 2B and S2c). Further, we estimated the intestinal barrier permeability by measuring serum concentrations of fluorescein isothiocyanate (FITC)-dextran which was gavaged orally to these mice. A twelve fold increase in FITC-dextran in the serum of the wild type animals was seen, while the *rela*$^{\Delta hep}$*stat3*$^{\Delta hep}$ mice showed substantially lower, five-fold increase (Figure 2D).

We also examined *rela*$^{\Delta hep}$*stat3*$^{\Delta hep}$ mice for the epithelial architecture and mucin expression in colon by following histological features and expression of colitogenic markers. DSS treatment led to extensive disruption of the intestinal crypts and depletion of the mucin layer in wildtype mice, accompanied by submucosal leukocyte infiltration. In contrast, *rela*$^{\Delta hep}$*stat3*$^{\Delta hep}$ mice showed substantially attenuated epithelial changes along with minimal erosion of mucin layers (Figure 2C). RT-qPCR analysis revealed that DSS treatment of wildtype mice triggered a two and a half-fold and two-fold reduction in the colonic abundance of enterocyte markers, tight junction 1 (tjp1) and occludin (ocln), respectively (Figure 2E). Similarly, we noticed a four-fold and two-fold decrease in the colonic abundance of goblet cell markers, mucins-2 and trefoil factor 3 (tff3), respectively, in wildtype mice upon DSS treatment. Except for a moderate decrease in the Tjp1 mRNA level, none of these mRNAs were downregulated upon DSS treatment in *rela*$^{\Delta hep}$*stat3*$^{\Delta hep}$ mice. Taken together these studies reveal intriguing observations wherein the absence of Rela and Stat3 in hepatocytes protects mice from DSS-induced colitis.

Induced hepatic expression of Rela and Stat3 stimulates primary bile acid synthesis pathway genes.

To dissect the mechanism underlying the resistant phenotype displayed by hepatocyte-specific *rela*$^{\Delta hep}$*stat3*$^{\Delta hep}$ mice, we performed global transcriptome studies from liver tissues of treated/untreated *rela*$^{\Delta hep}$*stat3*$^{\Delta hep}$ strain and their wild type littermates. Unsupervised clustering of transcriptomic data using PCA tool segregate wildtype and *rela*$^{\Delta hep}$*stat3*$^{\Delta hep}$ mice samples subjected to DSS treatment (Figure 3A). Notably, untreated mice from wildtype and *rela*$^{\Delta hep}$*stat3*$^{\Delta hep}$ cluster together in the PCA plot. Comparative pathway enrichment analysis using GO terms for differentially expressed genes in the liver upon DSS treatment between wildtype and *rela*$^{\Delta hep}$*stat3*$^{\Delta hep}$ mice showed differences in the acute phase responses, bile acid metabolic processes, response to ER stress, and one-carbon metabolism (Figure 3B). BA dysmetabolism has been reported in IBD patients by several studies and is also recapitulated in the mice models [22, 23]. The consensus thesis is that the levels of secondary BAs are lower, primary BAs are elevated because of impairment of microbiota-mediated deconjugation and transformation activities. Concordantly, our analysis from colonic biopsies of IBD subjects also showed elevated levels for primary BAs (Figure 3C).

BAs are synthesized in hepatocytes through the classical and alternate pathways catalyzed by a set of P450 enzymes (Figure 3D). Cholic acid (CA) and chenodeoxycholic acid (CDCA) are primary bile acids and are conjugated to either glycine (predominantly in humans) or taurine (mainly in mice). Transcriptomics data strikingly showed downregulation of Cyp7b1 in the *rela*$^{\Delta hep}$*stat3*$^{\Delta hep}$ mice and the other biosynthesis enzymes also follow a similar trend (Figure S3a). Our RT-qPCR analyses substantiated that in comparison to DSS-treated wildtype mice, DSS-treated *rela*$^{\Delta hep}$*stat3*$^{\Delta hep}$ mice expressed a reduced level of mRNAs encoding primary bile acid synthesis pathway enzymes Cyp7a1, Cyp8b1, Cyp27a1 and Cyp7b1 in the liver (Figure 3E). Thus, our data propose a new hypothesis that hepatic Rela and Stat3 instruct a gene program in the liver of colitogenic mice that supports the expression of mRNAs encoding primary BA metabolism enzymes.

Reducing the levels of primary bile acids dampened intestinal inflammation in colitogenic *rela*$^{\Delta hep}$*stat3*$^{\Delta hep}$ mice.

To investigate if the altered hepatic gene expression led to a change in the abundance of primary bile metabolites in *rela*$^{\Delta hep}$*stat3*$^{\Delta hep}$ mice, we performed a targeted metabolomic study using LC-MS. Apart from measuring CA and CDCA, we also measured the level of CDCA-derived bile metabolites, namely ursodeoxycholic acid and α- and β-muricholic acid which are specifically produced in mice [24]. Our analyses revealed the abundance of cholic acid in the liver, which was approximately seven-fold less in DSS-treated *rela*$^{\Delta hep}$*stat3*$^{\Delta hep}$ mice compared to their wildtype counterparts (Figure 4A). Likewise, we captured a close to ten-fold decrease in the hepatic level of CDCA in DSS-treated knockout mice. A substantially reduced levels of ursodeoxycholic acid and α-muricholic acid. We further compared DSS-treated wildtype and *rela*$^{\Delta hep}$*stat3*$^{\Delta hep}$ mice for the colonic abundance of these bile acids. Consistent with the levels observed in the liver, we found a significantly reduced accumulation of both CA and CDCA in the colon of DSS-treated *rela*$^{\Delta hep}$*stat3*$^{\Delta hep}$ mice. The difference between wildtype and knockout mice was substantially more marked for CDCA (Fig 4B).

CDCA has been reported to engage the NLRP3 inflammasome, causing liver inflammation during cholestasis [25]. Further, ex vivo experiments have shown that CDCA induces pro-inflammatory cytokine secretion by intestinal epithelial cells [26]. Because we noticed an altered abundance of these primary bile acids in *rela*$^{\Delta hep}$*stat3*$^{\Delta hep}$ mice, we asked if DSS treatment dampened the pro-inflammatory response in these knockouts. Indeed, compared to DSS-treated wildtype mice, DSS-treated knockout mice presented with substantially reduced level of mRNAs encoding key pro-inflammatory cytokines, namely Il1b, Tnfa, and Il6 (Fig 4C). Consistent with the less inflamed intestinal milieu, *rela*$^{\Delta hep}$*stat3*$^{\Delta hep}$ mice also displayed a diminished frequency of

inflammatory effector immune cells in the colitogenic gut (Fig 4D). Confocal microscopy-based analyses of stained colon sections depicted a close to five-fold reduction in the recruitment of Ly6G+ cells, including neutrophils and monocytes, F4/80+ macrophages, and CD11c+ including macrophages and the dendritic cells in DSS-treated knockout mice, compared to their wildtype counterparts (Figure 4D and S4a). Taken together, we propose that a reduced accumulation of primary bile acids alleviates experimental colitis in *rela*$^{\Delta hep}$*stat3*$^{\Delta hep}$ mice.

Supplementing chenodeoxycholic acid restores colitogenic sensitivity of *rela*$^{\Delta hep}$*stat3*$^{\Delta hep}$ mice.

Recent studies have highlighted the role of CA in potentiating intestinal damage by impairing Lgr5^{+} intestinal stem cells. However, the role of CDCA in regulating intestinal inflammation in colitogenic mice remains unclear. Therefore we supplemented CDCA intraperitoneally daily for six days during DSS treatment in the wildtype or *rela*$^{\Delta hep}$*stat3*$^{\Delta hep}$ mice and scored the DAI. The optimum concentration of CDCA was determined by performing a dose-response curve. Mere daily supplementation of CDCA at the concentration of 10 mg/kg of body weight did not induce a colitogenic phenotype in either wildtype or *rela*$^{\Delta hep}$*stat3*$^{\Delta hep}$ mice even after six days (Fig S5 a-c). Moreover, the DAI of wildtype mice treated with both DSS and CDCA showed no change (Figure 5A). On the other hand, CDCA supplementation of the DSS-treated *rela*$^{\Delta hep}$*stat3*$^{\Delta hep}$ mice showed DAI equivalent to wildtype DSS-treated mice with concomitant supplementation of colon length shortening (Figure 5A and Figure 5B). Histological analyses of DSS treated colon sections further substantiated that CDCA supplementation together with DSS treatment was sufficient for imparting damage to the colonic crypts of the colitis resistant *rela*$^{\Delta hep}$*stat3*$^{\Delta hep}$ mice (Figure 5C). Consistent to the observed intestinal pathologies, bile acid supplementation also triggered a drastic reduction in the colonic abundance of mRNAs encoding the junctional proteins Tjp1 and Ocln as well as Muc2 in DSS-treated *rela*$^{\Delta hep}$*stat3*$^{\Delta hep}$ mice (Figure 5D). Concurrently, bile acid-supplemented *rela*$^{\Delta hep}$*stat3*$^{\Delta hep}$ mice show prominently upregulated expression of genes encoding the pro-inflammatory cytokines Il1b, Tnfa and Il6 upon DSS treatment, compared to those treated with DSS alone (Figure 5E). Thus, we conclude that RelA and Stat3-driven accumulation of CDCA aggravates intestinal inflammation induced damage during experimental colitis.

Discussion

IBD are a heterogenous group of chronic inflammatory intestinal disorders that are influenced by environmental cues, intestinal dysbiosis and the local immune responses [27, 28]. Chronic intestinal inflammation remodels the permeability barrier resulting in leakage of microbial

components, including LPS, through the portal circulation thereby engaging extraintestinal organs such as the liver. Conventional treatment regimen for IBD involves the aminosalicylates, corticosteroids and anti-TNF agents to counter bowel inflammation [29]. Systemic effects are only addressed upon worsening of symptoms [30]. To improve the clinical management of IBD, thus there is a need to identify targets and mechanisms that can concurrently address other associated causes. In this study, we reveal the surprising role of hepatic rela-stat3 in regulating biosynthesis of primary bile acids, whose activation augments intestinal inflammation.

Lipopolysaccharides (LPS), one of the key components of microbial products, is known to induce inflammasome assembly by NF-κB/Lipocalin2-dependent axis in macrophages of colitogenic mice [31]. Similarly, LPS mediated non-canonical Stat3 activation through TLR4 ligand reprograms metabolic and inflammatory pathways in macrophages [17]. In the acute DSS-induced colitis model, release of LPS and other endotoxins would first activate kupffer cells of the liver, which then progressively triggers response in relatively quiescent hepatocytes [10]. We argued that Stat3-NF-κB signaling may be of specific significance, since these pathways in hepatocytes are known to control secretion of hepatic factors. We indeed observed activation of the canonical arm of the NF-κB signaling pathway with RelA phosphorylation at Ser536 residue following DSS treatment. Interestingly, non-canonical Stat3 activation was detected with Ser727 phosphorylation preceding the phosphorylation of canonical Tyr705 residue. To understand the significance of these signaling pathways of hepatocytes in the context of disease outcomes and its functional consequence in disease management, we subjected the single and double hepatocyte-specific knockout mice to DSS treatment. Surprisingly, the $rela^{\Delta hep}stat3^{\Delta hep}$ mice had attenuated disease activity index as well as diminished inflammatory response in the gut. Previous studies wherein attenuation of colitogenic phenotype have been reported are for the gut-resident cells [32, 33, 34, 35]. This study is amongst the first such, where ablation of genes in a distal organ - the liver - ameliorates colitis.

We then investigated the mechanisms underlying signaling networks in the liver that promote the colitis phenotype. Previously, hepatic Rela and Stat3 have been reported to act in a cooperative manner to render protection against pulmonary infection, by eliciting an acute phase response, which enhances the pulmonary immune response [36, 37]. We observe similar hepatic functions of Rela and Stat3 that amplify the immune response during experimental colitis, aggravating intestinal pathologies. Our unbiased transcriptome analysis of the liver genes revealed several metabolic and immune pathways to be altered in colitogenic mice. Amongst these, biosynthesis of primary BAs prompted our immediate attention. The primary bile acids are known to have inflammatory activity and the cardinal paradigm in IBD is the decreased levels of secondary bile acid [38, 39]. This has been attributed to the altered gut microflora that are known to

convert primary BAs into secondary BAs. It is important to note that most of these studies are carried out with fecal samples and a recent study that profiled the human intestinal environment under physiological conditions concluded that stool-based measurements do not reflect the true composition of BAs along the intestinal tracts. Intestinal samples were dominated by primary BAs, whereas stool samples were dominated by secondary BAs [40]. We therefore measured the intestinal BAs in IBD subjects by using mucosal biopsies and observed elevated levels of primary BAs in the IBD subjects as compared to non-IBD subjects.

Analysis of colitogenic mice intestinal samples also revealed enhanced primary BAs using mass spectrometry based measurements. We observe both CDCA and CA accumulate in the intestine and liver of colitogenic wild type mice when compared to knockout littermates. This accumulation of primary BA in both the intestine and liver is likely to be a consequence of increased biosynthesis in the liver and subsequent transport to the gut. Indeed, multiple primary bile synthesis pathway genes namely cyp7a1, cyp27a1, cyp7b1, and cyp8b1 were substantially upregulated in the liver. Our observation is contradictory to the recently published work by Gui et al which suggest that during IBD there is a downregulation of the biosynthesis machinery leading to reduced bile levels [41]. Currently we assume that these differences may arise due the dose of DSS, the time course of the experiment and the mice strain adapted for different studies leading to the difference in the transcriptional and metabolic landscape during IBD [41, 42 ,16] .

Conventionally the cyp450 enzymes involved in the bile acid biosynthesis pathway are known to be regulated by the FXR signaling cascade [43]. Our data suggest that RelA and Stat3 transcriptionally control these pathways under stress conditions. These two transcription factors have been known to collaborate in a variety of physiological and disease settings. Further studies would elucidate mechanistic understanding of how these hepatocyte-specific transcriptional regulatory circuitry drives hepatic bile synthesis during gastrointestinal abnormalities. Mutant mice that showed refractory behavior towards colitogensis, where mere supplementation of CDCA resulted in exacerbated colitis phenotype in the gut. Previous studies of increased CA has been attributed to colitis and CA was shown to limit the self-renewal capacity of intestinal stem cells leading to impaired intestinal restitution [42]. We now propose that increased synthesis and secretion of the primary bile acids orchestrates intestinal inflammation. It is increasingly important to understand how bile acid signaling networks are affected in distinct organs where the bile acid composition differs, and how these networks impact intestinal diseases. Our studies identify a new, important Rela-Stat3 network system of hepatocytes that could enable development of therapeutics that targets BA imbalance by suppressing host-specific stress-induced pathways.

Materials and Methods

Human Studies

All studies were approved by the All India Institute of Medical Science Ethics Committee for post-graduate research (Approval number – IECPG-270/22.04.2019). Biopsy specimens were collected from recto-sigmoidal or sigmoidal colon regions. Ulcerative colitis patients with mild-to-moderate disease activity (SCCAI: 3-9) were included in the IBD group. Subjects undergoing sigmoidoscopy for inspection of manifestations such as haemorrhoidal bleeds were included in the non-IBD group. Patients with severe disease activity, history of antibiotics or topical steroids in the past 4 weeks, pregnancy, comorbid illnesses and/or history of bowel surgery were excluded. These samples were immediately stored at -80 degrees Celsius in cryovials till further processing.

Animal Studies

All mouse strains were housed at the National Institute of Immunology (NII) and utilized adhering to the institutional guidelines (Approval number – IAEC 579/21). 5-7 week old C57BL/6 mice were used. Hepatocyte-specific knockout animals (Cre under albumin promoter) *rela*$^{\Delta hep}$, *stat3*$^{\Delta hep}$ and *rela*$^{\Delta hep}$*stat3*$^{\Delta hep}$ along with their Cre-negative (referred to as wild type in the text) littermates *rela*$^{fl/fl}$, *stat3*$^{fl/fl}$, and *rela*$^{fl/fl}$*stat3*$^{fl/fl}$ were generously gifted by Dr. Lee Quinton, School of Medicine, Boston University, Boston, MA, USA. Above mentioned knockout strains were crossed with their corresponding wildtype littermates to expand the colonies for experimental purposes at the small animal facility.

Induction and assessment of colitis in mice

As described earlier [44], 5-7 weeks old male/female (18-21 g body weight) mice of the indicated genotypes were randomly chosen for administered with 2% of DSS in drinking water for six days. Subsequently, body weight and disease activity were assessed for six days from the onset of DSS treatment. All experiments were performed using littermate mice cohoused for a week prior to the initiation of the experiments. The disease activity index was estimated based on stool consistency and rectal bleeding. The score was assigned as follows – 0 points were given for well-formed pellets, 1 point for pasty and semi-formed stool, 2 points for liquid stool, 3 points for bloody smear along with stool, and 4 points were assigned for bloody fluid/mortality. Mice with more than 30% loss of body weight were considered moribund, and euthanized. For specific experiments, mice were euthanized at the indicated days post-onset of DSS treatment, and colon tissues were collected.

10 mg/kg body weight of chenodeoxycholic acid dissolved in DMSO was injected via intraperitoneal route into mice as described earlier [45].

Histopathological studies

At day six of DSS treatment, mice with the indicated genotypes were euthanized, and the entire colon was excised. The colon length was measured from the rectum to the caecum. Subsequently, distal colons were washed with PBS, fixed in 10% formalin, and embedded in paraffin. 5µm thick tissue sections were generated from the inflamed region and stained with hematoxylin and eosin (H&E). Alternately, sections were stained with Alcian Blue for revealing mucin content. Images were acquired using Image-Pro6 software on an Olympus inverted microscope under a 20X objective lens. The severity of colitis was assessed by epithelial damage and infiltration of inflammatory immune cells in the submucosa of the colon.

For assessing intestinal permeability, FITC-dextran was orally gavaged to untreated or DSS-treated mice 6 hours prior to sera collection. Fluorescent based quantitation of sera samples were performed using CLARIOstar microplate reader (λ_{ex} : 490 nm and λ_{em}: 520 nm).

Confocal microscopy: sample preparation & analysis

Sample preparation: Distal colon samples were fixed in 10% formalin for 24 hrs. Fixed sections were embedded in paraffin and 5-µm based sections were generated using microtome. Deparaffinization of sections were achieved by snap heating followed by xylene wash, subsequently, these were rehydrated. Antigen retrieval was performed using a sodium citrate buffer (10mM, pH 6.0) at 95 degrees for 10 minutes and the slides were allowed to cool down. Further, these were rinsed in PBS, permeabilized for 5 min in 0.4% PBST, and blocked for 1 hour in 5% bovine serum albumin. These sections were stained with fluorescently conjugated antibodies listed in table 1 for overnight at 4 degree. Non-conjugated primary antibodies were incubated O/N at 4 degrees followed by incubation of conjugated secondary antibody for 2hrs. Subsequently, the slides were rinsed in PBS and incubated with DAPI for nuclear staining. Finally, slides were mounted using fluoroshield mounting media, and slides were analyzed under ZEISS LSM 980 confocal microscope at 40X (oil) magnification.

For analysis, the ratio between the signal of interest / DAPI was calculated for every field. Each dot represents the average ratio for 5 individual fields of interest. The plot is representative data from 3 biological replicates.

Gene expression studies

Total RNA was isolated using MN-NucleoSpin RNA (as per manufacturer's instructions) from the

liver and colon of untreated and DSS-treated animals of indicated genotypes. cDNA was synthesized using Takara cDNA synthesis kit as per manufacturer protocol. RT-qPCR was performed using PowerUp SYBR Green PCR master mix in ABI 7500 FAST instrument. Relative mRNA levels were quantitated and GAPDH was used as a control.

Further, RNA isolated from liver tissue was subjected to paired-end RNA-seq analysis after rRNA depletion, on Illumina platform 6000 at core facility of the CCMB, India. Twenty million unique RNA fragments were sequenced per sample and the average length of the sequenced reads was around 150bp. The RNA-seq raw data is available in the NIH National Center for Biotechnology Information GEO database as GSE243307. Quality control and sequence trimming was performed using fastp (v0.23.2). The trimmed paired-end reads were aligned to the mouse genomes (mm9) using the HISAT2 (v2.2.1) pipeline. Reads were assembled into transcripts using StringTie (v2.2.1). Annotation was conducted using aligned sequences and a GTF annotation file. The mapped reads were then used for generating the count table using StringTie (v2.2.1). We had a total of 51,610 entries in our dataset for which differential expression analysis was performed using the DEseq2 R package. Pathway enrichment was performed using the GO database and clusters were visualized using the R package ClusterProfiler.

Biochemical studies

Immunoblot analyses:

Tissue fragment (colon or liver) were homogenized in hand held douncer in SDS-RIPA buffer (50 mM Tris-HCl pH 7.5, 150 mM NaCl, 1 mM EDTA, 0.1% SDS, 1% Triton-X 100, 1 mM DTT, 1X Proteinase inhibitor, 1X Protease inhibitor). Subsequently these extracts were centrifuged and the supernatants were resolved by SDS-PAGE and transferred onto a PVDF membrane, and immunoblotting was performed using indicated antibodies. Blots were developed using Immobilon HRP substrate and images were acquired through ImageQuant Chemiluminescent imaging system (LAS 500). Band intensities were quantified in ImageJ.

Targeted Metabolomics:

Lipid pools were extracted by a two-step liquid-liquid extraction protocol as described previously [46]. Specific weight of the murine tissue was homogenized in methanol twice using 1.0 mm Zirconium beads. Extracted tissue pellets were subjected to chloroform extraction using a bath sonicator twice. The methanol and chloroform fractions were pooled and evaporated using speed-vac. Samples were added with 150ul MeOH, vortexed, sonicated and filtered (0.45 µm) for further analysis. A triple quadruple mass spectrometer (Waters, Milford, MA,USA) recorded MS and MS/MS spectra using electrospray ionization (ESI) in negative ion (NI) mode. Waters Acquity

UPLC system was connected to the triple-quadrupole mass spectrometer. Analytical separations of the mixture of specific primary BAs were performed on the UPLC system using an ACQUITY UPLC C18 (1.6 mm 1*150 mm) analytical column.

Untargeted Metabolomics:

5mg of biopsy material was transferred to pre-chilled homogenizer vials, mixed with 80% methanol and subjected to 3 rounds of homogenization, each with 2 cycles of 30sec. The homogenate was centrifuged at 14000 g for 20 min at 4 degrees Celsius and thereafter dried overnight in Speed Vac. At the time of sample run the samples were resuspended in 15% ACN for Reverse Phase Chromatography, and LC/MS was performed on ThermoFisher Orbitrap Fusion Tribrid Mass Spectrometer.

Statistical analysis

Quantified data for 3-6 mice replicates were plotted as mean ± SEM (represented as error bars). Unless otherwise mentioned, unpaired two-tailed Student's t-test and one-way Anova was used for calculating statistical significance in data sets involving two groups and multiple groups respectively.

Acknowledgments

Acknowledgements: We thank Dr. Lee Quinton for providing us with hepatocyte specific knockout animals for *rela* and/or *stat3* for carrying out this study; Dr. Devram S. Ghorpade, NII, New Delhi for discussions; Next Generation Sequencing (NGS) facility at CSIR-CCMB for the transcriptomic support; Mass Spectrometric facility at THSTI, Faridabad for the metablomic support; the Small Animal Facility at the National Institute of Immunology, New Delhi for support with mice providing the breeding and experimental support; the Department of Biotechnology (DBT) for institutional support provided to National Institute of Immunology.

Data and Material Availability:

The mice strain used have been gifted by Dr. Lee Quinton from Boston University and is available at the breeding facility at the National Institute of Immunology. All materials and reagents will be available on request. The transcriptomic data will be available online at GEO with accession id GSE243307. All codes used for the analysis is publically available and can also be provided upon request.

References

1. Tripathi, A. *et al.* The gut–liver axis and the intersection with the microbiome. *Nat. Rev. Gastroenterol. Hepatol.* **15**, 397–411 (2018).
2. Horst, A. K., Neumann, K., Diehl, L. & Tiegs, G. Modulation of liver tolerance by conventional and nonconventional antigen-presenting cells and regulatory immune cells. *Cell. Mol. Immunol.* **13**, 277–292 (2016).
3. Kobayashi, T., Iwaki, M., Nakajima, A., Nogami, A. & Yoneda, M. Current Research on the Pathogenesis of NAFLD/NASH and the Gut-Liver Axis: Gut Microbiota, Dysbiosis, and Leaky-Gut Syndrome. *Int. J. Mol. Sci.* **23**, (2022).
4. Bailey, M. A. *et al.* Dietary fiber intake and fecal short-chain fatty acid concentrations are associated with lower plasma lipopolysaccharide-binding protein and inflammation. *American Journal of Physiology-Gastrointestinal and Liver Physiology* (2023) doi:10.1152/ajpgi.00176.2021.
5. Tilg, H., Adolph, T. E. & Trauner, M. Gut-liver axis: Pathophysiological concepts and clinical implications. *Cell Metab.* **34**, 1700–1718 (2022).
6. Kessoku, T. *et al.* The Role of Leaky Gut in Nonalcoholic Fatty Liver Disease: A Novel Therapeutic Target. *Int. J. Mol. Sci.* **22**, (2021).
7. Cappello, M. *et al.* Liver Function Test Abnormalities in Patients with Inflammatory Bowel Diseases: A Hospital-based Survey. *Clin. Med. Insights Gastroenterol.* **7**, 25–31 (2014).
8. Gaspar, R., Branco, C. C. & Macedo, G. Liver manifestations and complications in inflammatory bowel disease: A review. *World J. Hepatol.* **13**, 1956–1967 (2021).
9. Yamada, T. *et al.* Kupffer-cell depletion attenuates colonic and extracolonic granulomatous inflammation in chronic colitis. *J. Lab. Clin. Med.* **142**, 268–277 (2003).
10. Taniki, N. *et al.* Intestinal barrier regulates immune responses in the liver via IL-10-producing macrophages. *JCI Insight* **3**, (2018).
11. Kwon, J., Lee, C., Heo, S., Kim, B. & Hyun, C.-K. DSS-induced colitis is associated with adipose tissue dysfunction and disrupted hepatic lipid metabolism leading to hepatosteatosis and dyslipidemia in mice. *Sci. Rep.* **11**, 5283 (2021).
12. Zhu, L. *et al.* Multi-Omics Analysis of the Gut-Liver Axis Reveals the Mechanism of Liver Injury in Colitis Mice. *Front. Immunol.* **12**, 773070 (2021).
13. Yang, X. *et al.* Reductively modified albumin attenuates DSS-Induced mouse colitis through rebalancing systemic redox state. *Redox Biol* **41**, 101881 (2021).
14. Bosma, M. *et al.* FNDC4 acts as an anti-inflammatory factor on macrophages and improves colitis in mice. *Nat. Commun.* **7**, 11314 (2016).
15. Sun, R., Xu, C., Feng, B., Gao, X. & Liu, Z. Critical roles of bile acids in regulating intestinal

mucosal immune responses. *Therap. Adv. Gastroenterol.* **14**, 17562848211018098 (2021).

16. Zhou, X. *et al.* PPARα-UGT axis activation represses intestinal FXR-FGF15 feedback signalling and exacerbates experimental colitis. *Nat. Commun.* **5**, 4573 (2014).
17. Balic, J. J. *et al.* STAT3 serine phosphorylation is required for TLR4 metabolic reprogramming and IL-1β expression. *Nat. Commun.* **11**, 3816 (2020).
18. Sakai, J. *et al.* Lipopolysaccharide-induced NF-κB nuclear translocation is primarily dependent on MyD88, but TNFα expression requires TRIF and MyD88. *Sci. Rep.* **7**, 1428 (2017).
19. Zhou, Z., Xu, M.-J. & Gao, B. Hepatocytes: a key cell type for innate immunity. *Cell. Mol. Immunol.* **13**, 301–315 (2016).
20. Ahyi, A.-N. N. *et al.* Roles of STAT3 in protein secretion pathways during the acute-phase response. *Infect. Immun.* **81**, 1644–1653 (2013).
21. Chassaing, B., Aitken, J. D., Malleshappa, M. & Vijay-Kumar, M. Dextran sulfate sodium (DSS)-induced colitis in mice. *Curr. Protoc. Immunol.* **104**, 15.25.1–15.25.14 (2014).
22. Zhou, H. & Hylemon, P. B. Bile acids are nutrient signaling hormones. *Steroids* **86**, 62–68 (2014).
23. Bromke, M. A. & Krzystek-Korpacka, M. Bile Acid Signaling in Inflammatory Bowel Disease. *Int. J. Mol. Sci.* **22**, (2021).
24. Honda, A. *et al.* Regulation of bile acid metabolism in mouse models with hydrophobic bile acid composition. *J. Lipid Res.* **61**, 54–69 (2020).
25. Gong, Z. *et al.* Chenodeoxycholic acid activates NLRP3 inflammasome and contributes to cholestatic liver fibrosis. *Oncotarget* **7**, 83951–83963 (2016).
26. Horikawa, T. *et al.* Chenodeoxycholic Acid Releases Proinflammatory Cytokines from Small Intestinal Epithelial Cells Through the Farnesoid X Receptor. *Digestion* **100**, 286–294 (2019).
27. Ananthakrishnan, A. N. *et al.* Environmental triggers in IBD: a review of progress and evidence. *Nat. Rev. Gastroenterol. Hepatol.* **15**, 39–49 (2018).
28. de Souza, H. S. P. & Fiocchi, C. Immunopathogenesis of IBD: current state of the art. *Nat. Rev. Gastroenterol. Hepatol.* **13**, 13–27 (2016).
29. Gómez-Gómez, G. J., Masedo, Á., Yela, C., Martínez-Montiel, M. del P. & Casís, B. Current stage in inflammatory bowel disease: What is next? *World J. Gastroenterol.* **21**, 11282–11303 (2015).
30. Veloso, F. T. Extraintestinal manifestations of inflammatory bowel disease: do they influence treatment and outcome? *World J. Gastroenterol.* **17**, 2702–2707 (2011).
31. Kim, S. L., Shin, M. W. & Kim, S. W. Lipocalin 2 activates the NLRP3 inflammasome via LPS-induced NF-κB signaling and plays a role as a pro-inflammatory regulator in murine

macrophages. *Mol. Med. Rep.* **26**, (2022).

32. Chawla, M. *et al.* An epithelial pathway exacerbates intestinal inflammation by supplementing latent RelA dimers to the canonical NF-κB module. *Proc. Natl. Acad. Sci. U. S. A.* **118**, (2021).
33. Shi, Y., Liu, Z., Cui, X., Zhao, Q. & Liu, T. Intestinal vitamin D receptor knockout protects from oxazolone-induced colitis. *Cell Death Dis.* **11**, 461 (2020).
34. Weisser, S. B. *et al.* SHIP-deficient, alternatively activated macrophages protect mice during DSS-induced colitis. *J. Leukoc. Biol.* **90**, 483–492 (2011).
35. Bessman, N. J. *et al.* Dendritic cell-derived hepcidin sequesters iron from the microbiota to promote mucosal healing. *Science* **368**, 186–189 (2020).
36. Quinton, L. J. *et al.* Hepatocyte-specific mutation of both NF-κB RelA and STAT3 abrogates the acute phase response in mice. *J. Clin. Invest.* **122**, 1758–1763 (2012).
37. Hilliard, K. L. *et al.* The lung-liver axis: A requirement for maximal innate immunity and hepatoprotection during pneumonia. *Am. J. Respir. Cell Mol. Biol.* **53**, 378–390 (2015).
38. Sinha, S. R. *et al.* Dysbiosis-induced secondary bile acid deficiency promotes intestinal inflammation. *Cell Host Microbe* **27**, 659–670.e5 (2020).
39. Yang, M. *et al.* Bile Acid-Gut Microbiota Axis in Inflammatory Bowel Disease: From Bench to Bedside. *Nutrients* **13**, (2021).
40. Shalon, D. *et al.* Profiling the human intestinal environment under physiological conditions. *Nature* **617**, 581–591 (2023).
41. Gui, W. *et al.* Colitis ameliorates cholestatic liver disease via suppression of bile acid synthesis. *Nat. Commun.* **14**, 3304 (2023).
42. Chen, L. *et al.* Hepatic cytochrome P450 8B1 and cholic acid potentiate intestinal epithelial injury in colitis by suppressing intestinal stem cell renewal. *Cell Stem Cell* **29**, 1366–1381.e9 (2022).
43. Eloranta, J. J. & Kullak-Ublick, G. A. The Role of FXR in Disorders of Bile Acid Homeostasis. *Physiology* (2008) doi:10.1152/physiol.00020.2008.
44. Kiesler, P., Fuss, I. J. & Strober, W. Experimental Models of Inflammatory Bowel Diseases. *Cell Mol Gastroenterol Hepatol* **1**, 154–170 (2015).
45. Ward, J. B. J. *et al.* Ursodeoxycholic acid and lithocholic acid exert anti-inflammatory actions in the colon. *Am. J. Physiol. Gastrointest. Liver Physiol.* **312**, G550–G558 (2017).
46. Gaikwad, N. W. Bileome: The bile acid metabolome of rat. *Biochem. Biophys. Res. Commun.* **533**, 458–466 (2020).

Figure and Figure Legends

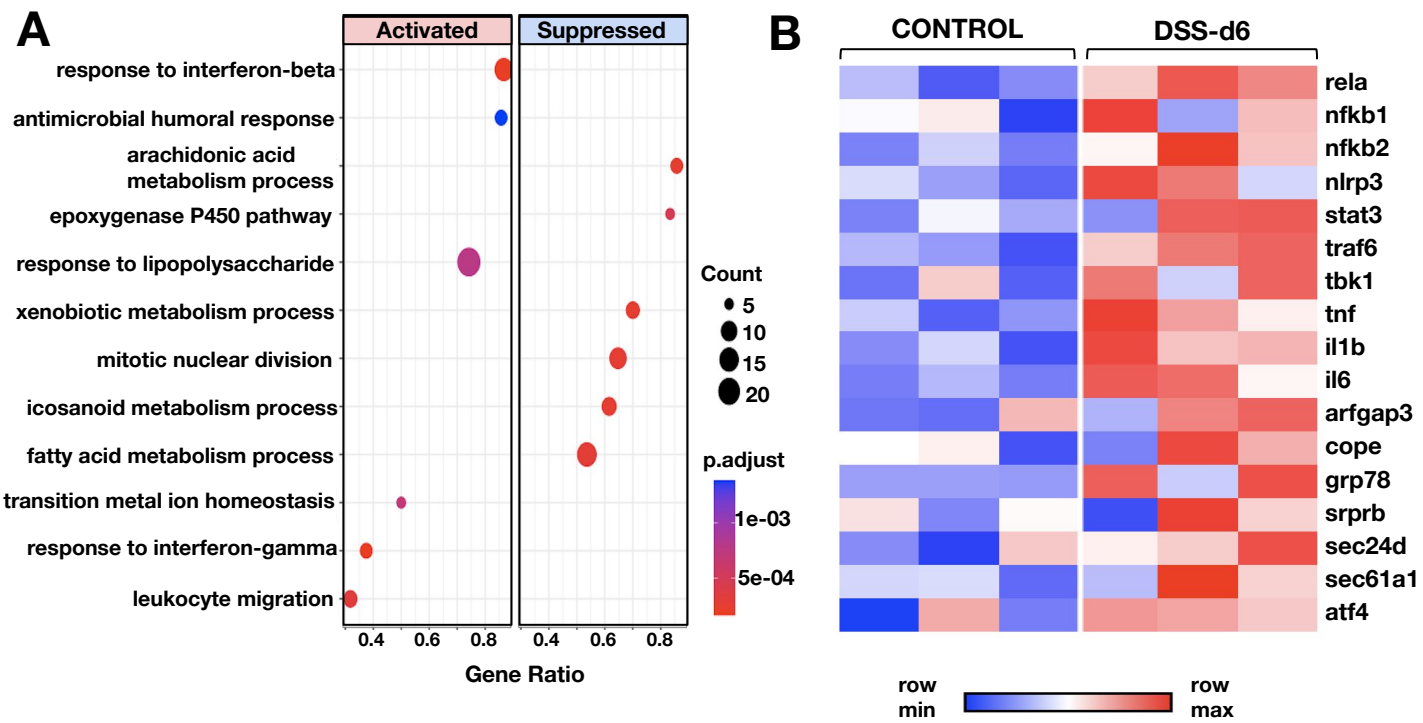

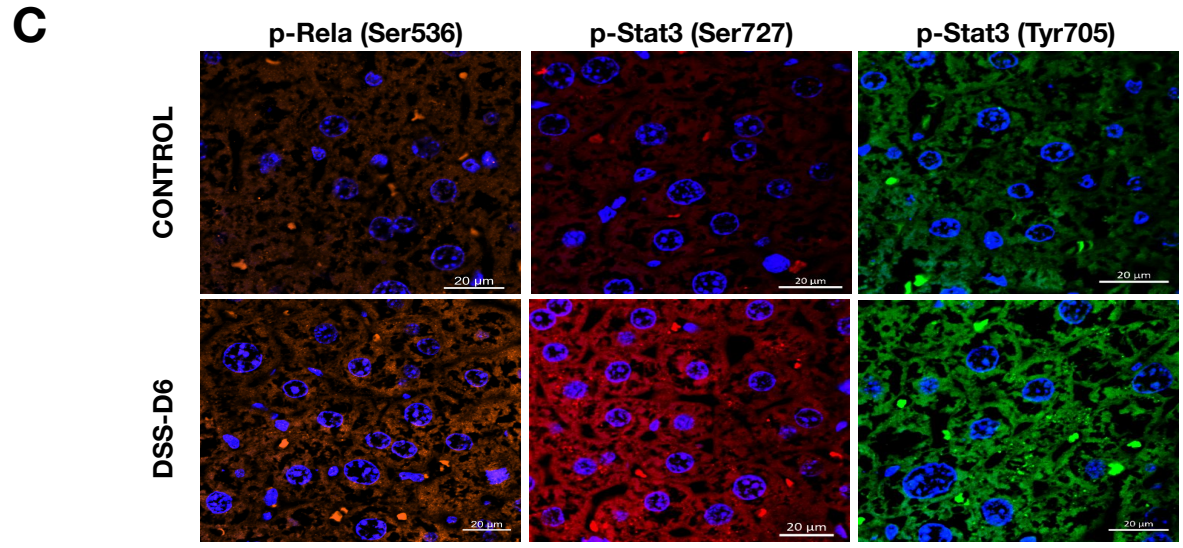

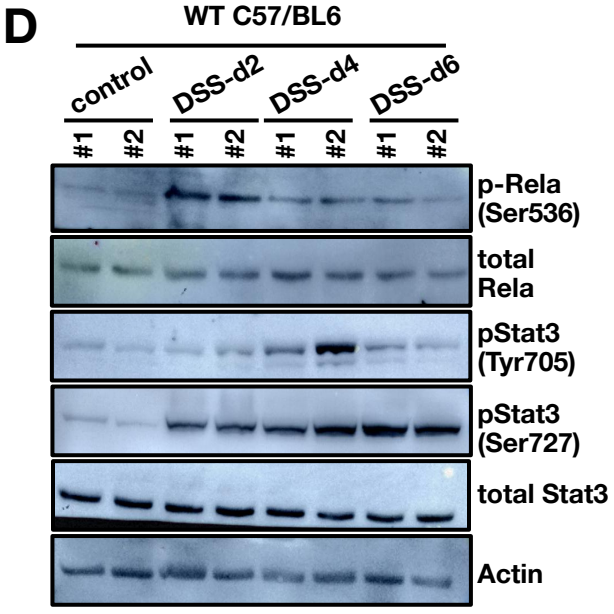

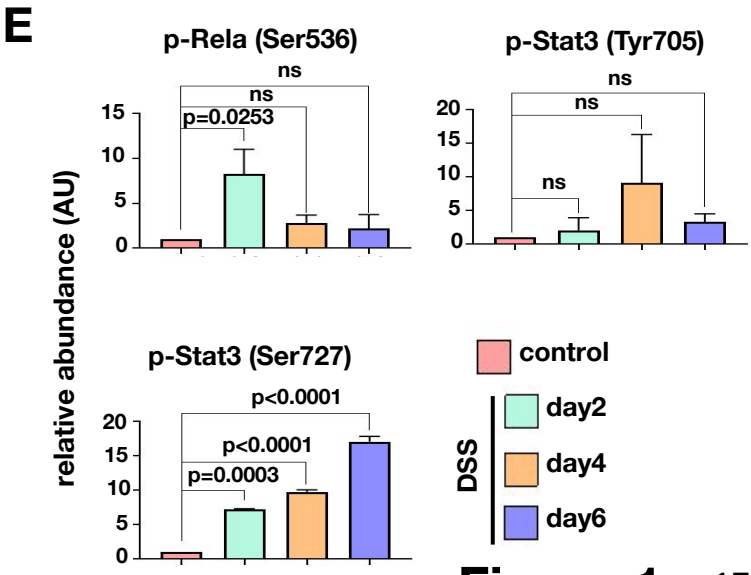

Figure 1

Figure 1: Initiation of colitis in mice lead to hepatic Rela and Stat3 activation. (A) GO pathway enrichment analysis was done for DEGs with adjusted p-value < 0.05 on days 6 post DSS treatment. Bubble plot depicts the enrichment of pathways on day 6 for different genotypes, where the coordinate on x-axis represents gene ratio, size of bubble represents the gene count and colour represents the p-value. **(B)** Heatmap represents normalized transcript count of the Rela and Stat3 pathway obtained from the RNA-seq experiment of three biological replicates. Scale is normalized across each row and colour from blue to red represents minimum and the maximum values respectively. **(C)** Representative confocal microscopy images show Rela and Stat3 activation in untreated and 6 days DSS-treated liver tissue of C57BL/6 mice. Blue, orange, red and green color represents represents the nuclei, p-Rela (Ser536), p-Stat3 (Ser727) and p-Stat3 (Tyr705). Images were taken at 40X. Scale is 20 μm. **(D)** Western blot revealing the abundance of total Rela and total Stat3, and their phosphorylated functionally active forms, in the liver extracts prepared from wildtype C57BL/6 mice either left untreated or subjected to DSS treatment for two, four and six days. **(E)** The signal intensity of bands corresponding to the indicated phosphorylated proteins was quantified from western blots, normalized against beta-actin, and presented as a bar plot. The data represent the means of three biological replicates ± SEM.

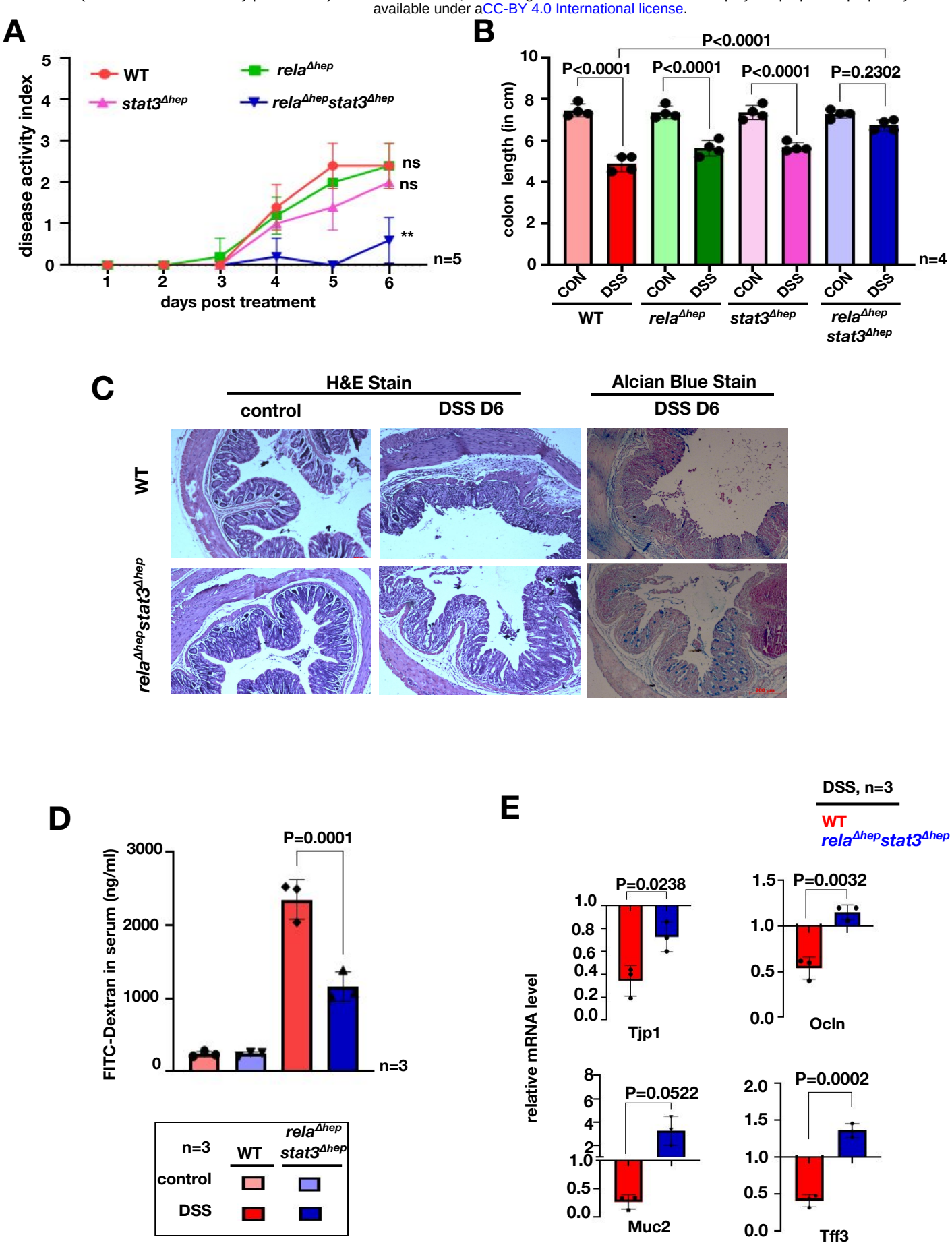

Figure 2

Figure 2: ***rela*** **and** ***stat3*** **deficiency in hepatocytes ameliorates DSS-induced acute colitis in mice. (A)** Line plot charting disease activity index of wild type, $rela^{\Delta hep}$, $stat3^{\Delta hep}$ and $rela^{\Delta hep}stat3^{\Delta hep}$ littermate mice subjected to treatment with 2% DSS for six days. **(B)** Bar plot revealing colon length measured on day six post-onset of DSS treatment of mice of the indicated genotypes. Untreated mice were used as controls. **(C)** Bar plot quantifying gut permeability. Briefly, untreated and DSS-treated wildtype and $rela^{\Delta hep}stat3^{\Delta hep}$ mice were orally gavaged with FITC-dextran and serum concentration of FITC was measured in another six hours. **(D)** Colon sections from untreated and DSS-treated mice of the indicated genotypes were examined for histological features involving H&E staining [upper panel] and alcian blue staining [lower panel]. Data were obtained in 10X magnification and represent three experimental replicates; two fields per section and a total of three sections from each set were examined. **(E)** RT-qPCR revealing the relative abundance of the indicated mRNAs encoding broadly IEC-specific or goblet cell-specific markers in untreated or DSS-treated mice of the indicated genotypes.

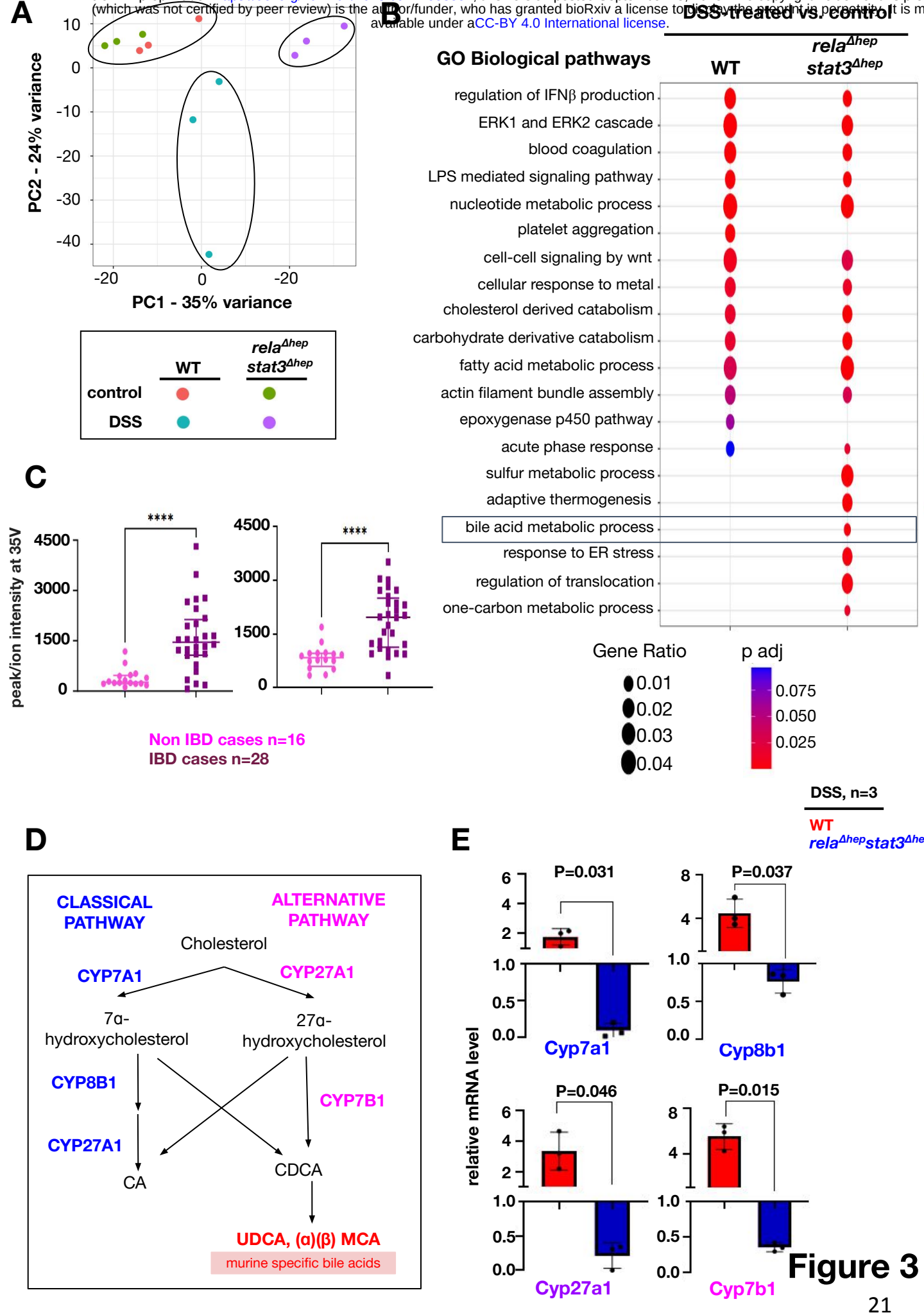

Figure 3

Figure 3: **Charting hepatic gene expressions in colitogenic wildype and *rela*$^{\Delta hep}$*stat3*$^{\Delta hep}$ mice. (A)** PCA plot illustrating the hepatic transcriptome, identified through global RNA-seq analyses, of untreated or DSS treated wildtype and *rela*$^{\Delta hep}$*stat3*$^{\Delta hep}$ mice (n=3). DSS treatment was carried out for six days. **(B)** Bubble plot depicting the relative enrichment of GO biological terms among genes differentially expressed in wildtype or *rela*$^{\Delta hep}$*stat3*$^{\Delta hep}$ mice. The gene ratio for a given term and the adjusted p value associated with the enrichment score has been presented for the individual genetic backgrounds. **(C)** Dot plot of dinor-cholic acid and dinor-chenodeoxycholic acid detected in an untargeted LC-MS based quantification of bile acid in the mucosal biopsy samples from IBD and Non-IBD patients. **(D)** Schematic presentation of classical and alternate pathways of bile synthesis in mice. CA, CDCA, MCA and UDCA represent cholic, chenodeoxycholic, muricholic and ursodeoxycholic acids, respectively. **(E)** RT-qPCR analyses comparing the hepatic abundance of indicated mRNAs encoding enzymes involved in bile metabolism in DSS-treated wildtype and *rela*$^{\Delta hep}$*stat3*$^{\Delta hep}$ mice (n=3).

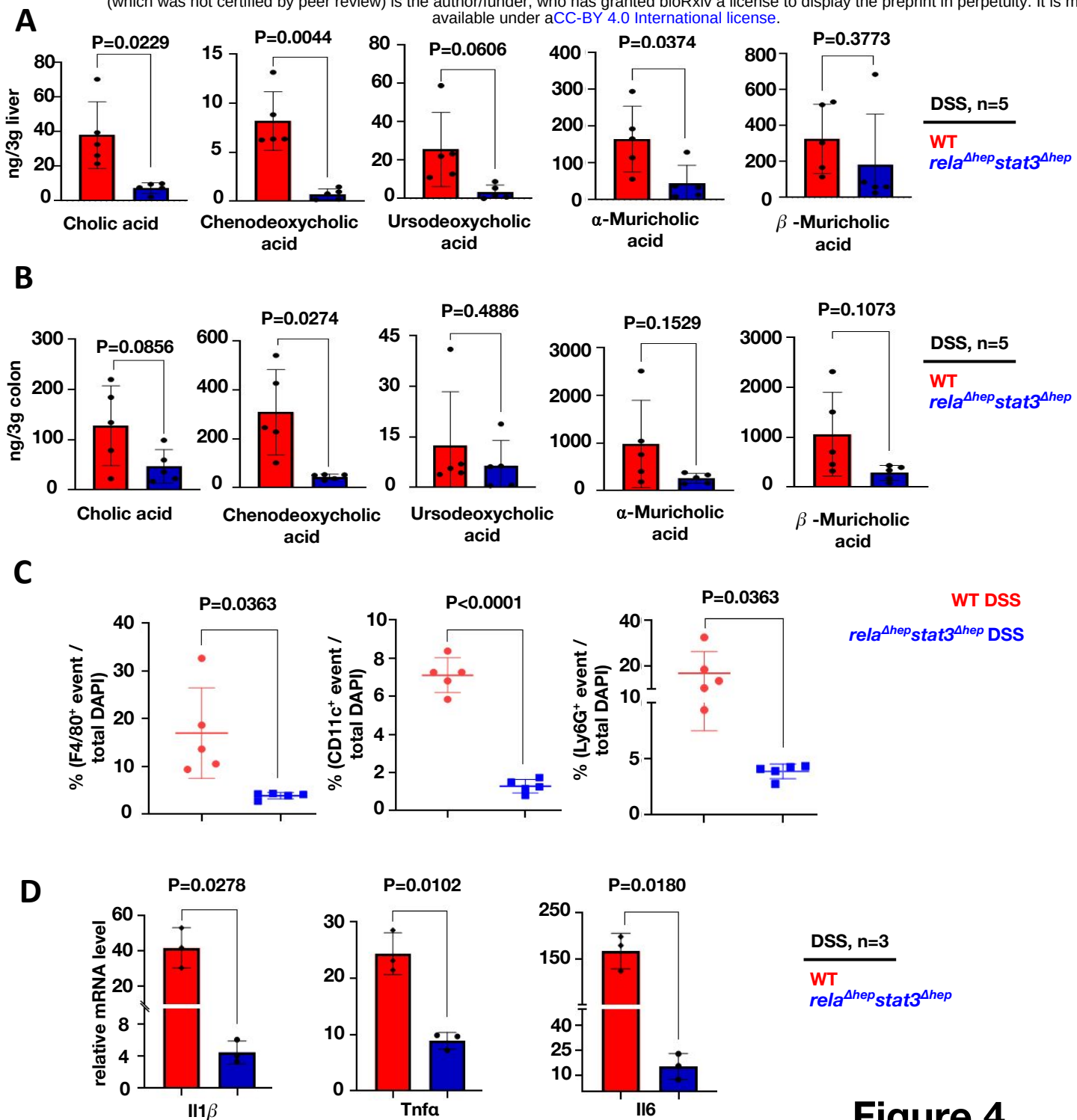

Figure 4

Figure 4: Altered accumulation of primary bile acids in *rela*$^{\Delta hep}$*Stat3*$^{\Delta hep}$ mice accompanies a less severe inflammatory signature in the colitogenic gut. Targeted LC-MS based quantification of primary bile acid in the liver **(A)** and the colon **(B)** of DSS-treated wildtype and *rela*$^{\Delta hep}$*stat3*$^{\Delta hep}$ mice (n=5). **(C)** RT-qPCR analyses comparing DSS-treated wildtype and *rela*$^{\Delta hep}$*stat3*$^{\Delta hep}$ mice for the colonic abundance of indicated mRNAs encoding pro-inflammatory cytokines (n=3). **(D)** Dot-plot representing the frequency of F4/80+, Ly-6G+ and CD11c+ cells among total DAPI-stained cells in the colon sections derived from DSS treated wildtype and *rela*$^{\Delta hep}$*stat3*$^{\Delta hep}$ mice.

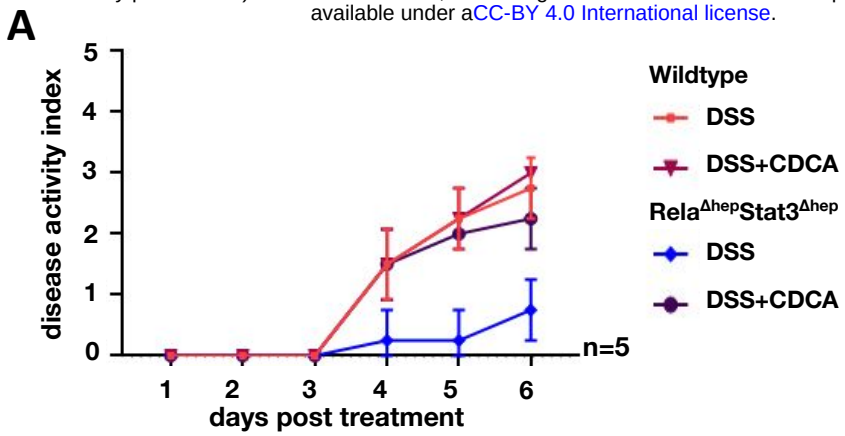

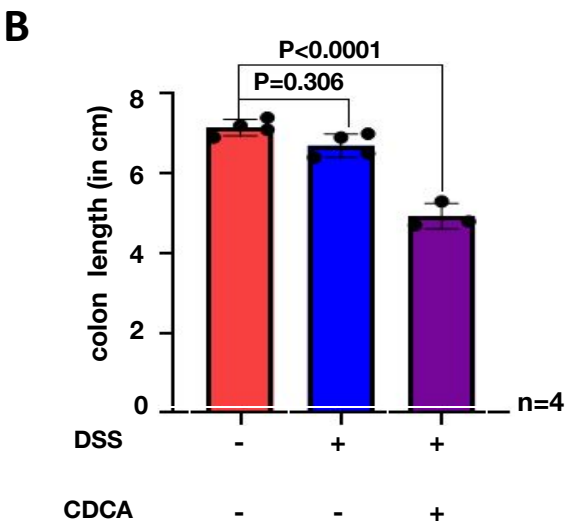

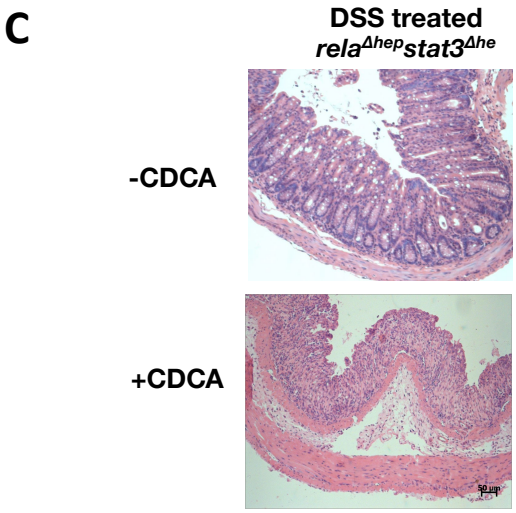

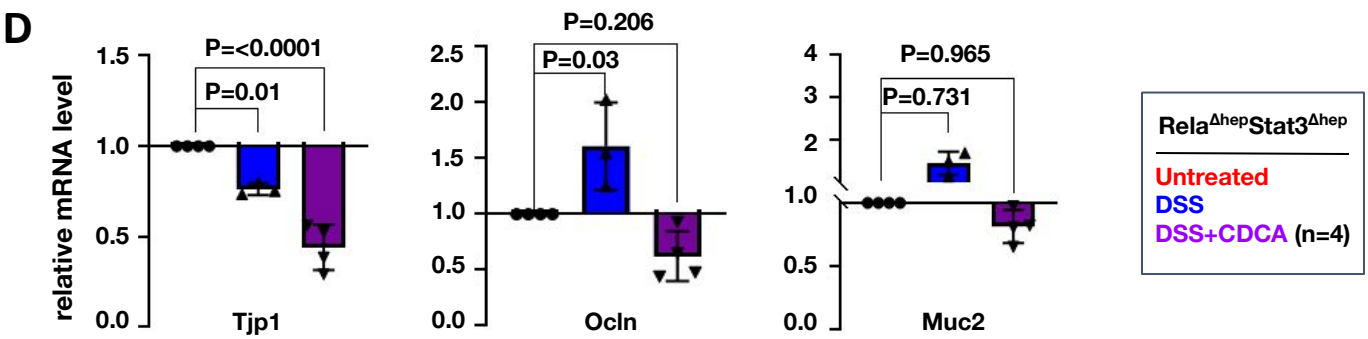

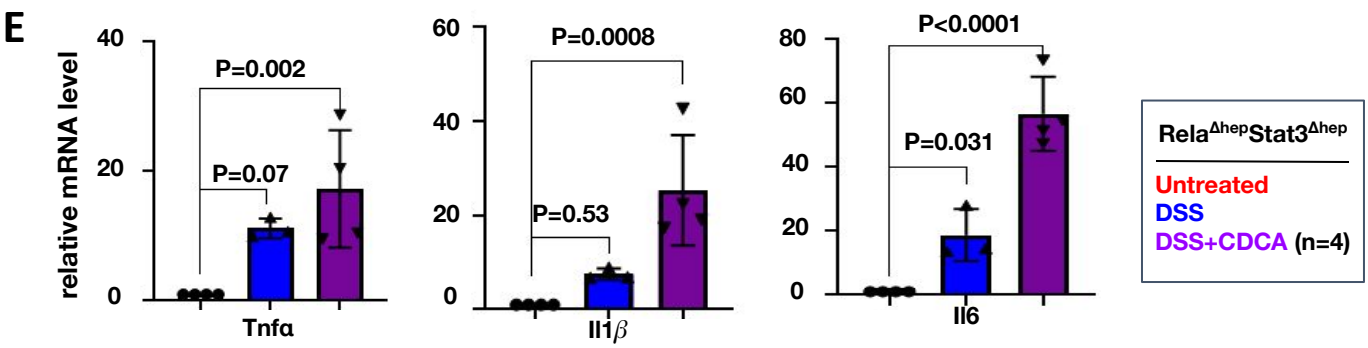

Figure 5

Figure 5: Supplementing Chenodeoxycholic acid restores the colitogenic sensitivity in *rela*$^{\Delta hep}$*stat3*$^{\Delta hep}$ mice. (A) Line plot charting the disease activity in a time course of wildtype and *rela*$^{\Delta hep}$*stat3*$^{\Delta hep}$ mice subjected to DSS treatment while being daily supplemented with 10 mg/kg CDCA. Mice devoid of CDCA supplementation were treated with DMSO as controls. **(B)** Bar plot comparing the colon length of *rela*$^{\Delta hep}$*stat3*$^{\Delta hep}$ mice subjected to DSS treatment for six days in the absence or presence of CDCA supplementation. **(C)** Similarly, colon sections from DSS-treated *rela*$^{\Delta hep}$*stat3*$^{\Delta hep}$ mice either not supplemented or supplemented with CDCA were examined by H&E staining. Data were obtained in 10X magnification and represent four experimental replicates. The data represent n = 3; a total of four sections from each set were examined. RT-qPCR analyses comparing the colonic abundance of indicated mRNAs encoding entrocytic markers **(D)** and pro-inflammatory cytokines **(E)** in mice subjected to DSS treatment for six days in the absence or presence of CDCA supplementation (n=4). Untread mice were used as controls.

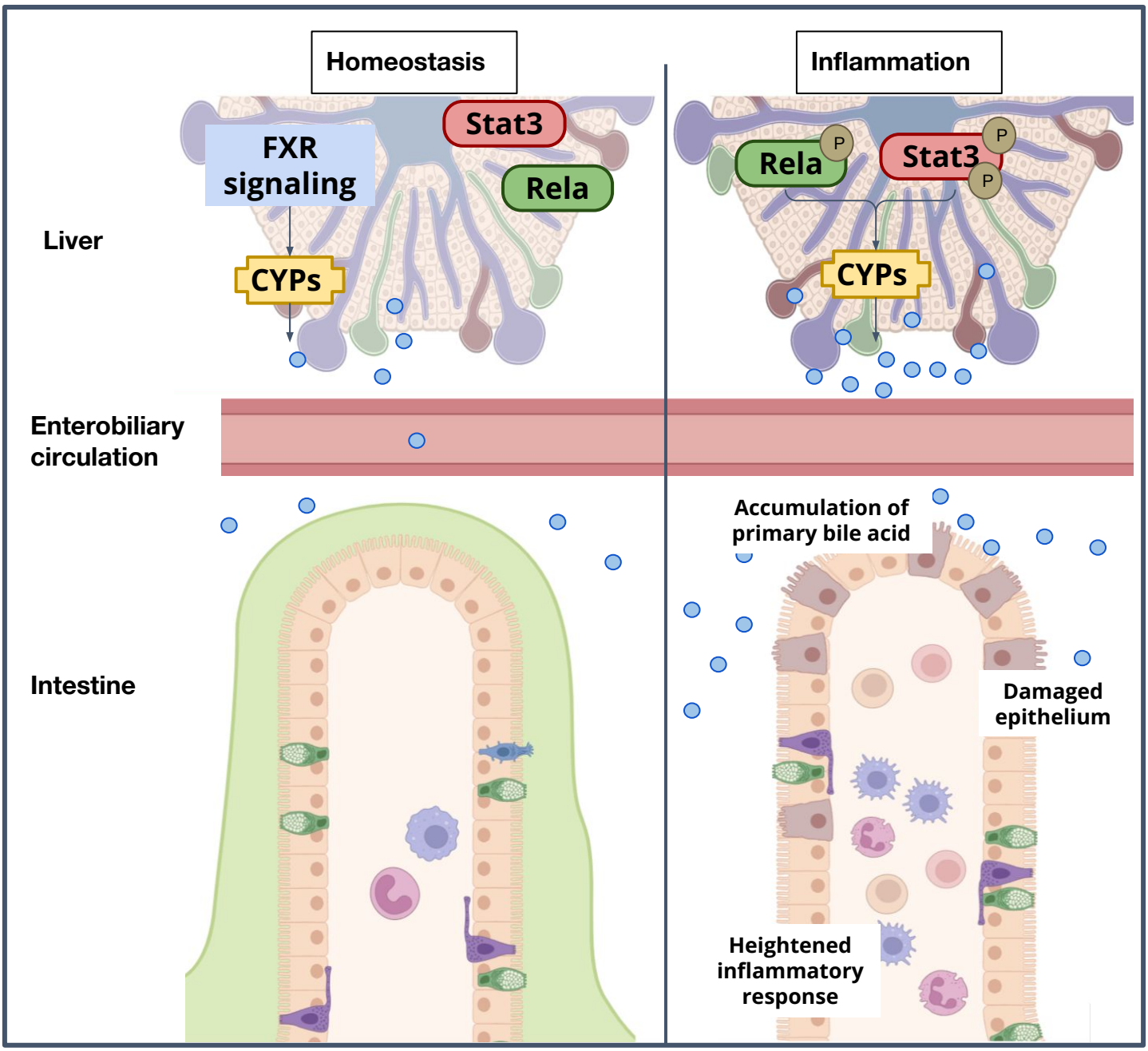

Figure 6

Figure 6: A model depicting the immuno-metabolic network linking the inflammation induced hepatic signaling pathway to intestinal pathologies in mice.

Supplementary Figures and Tables

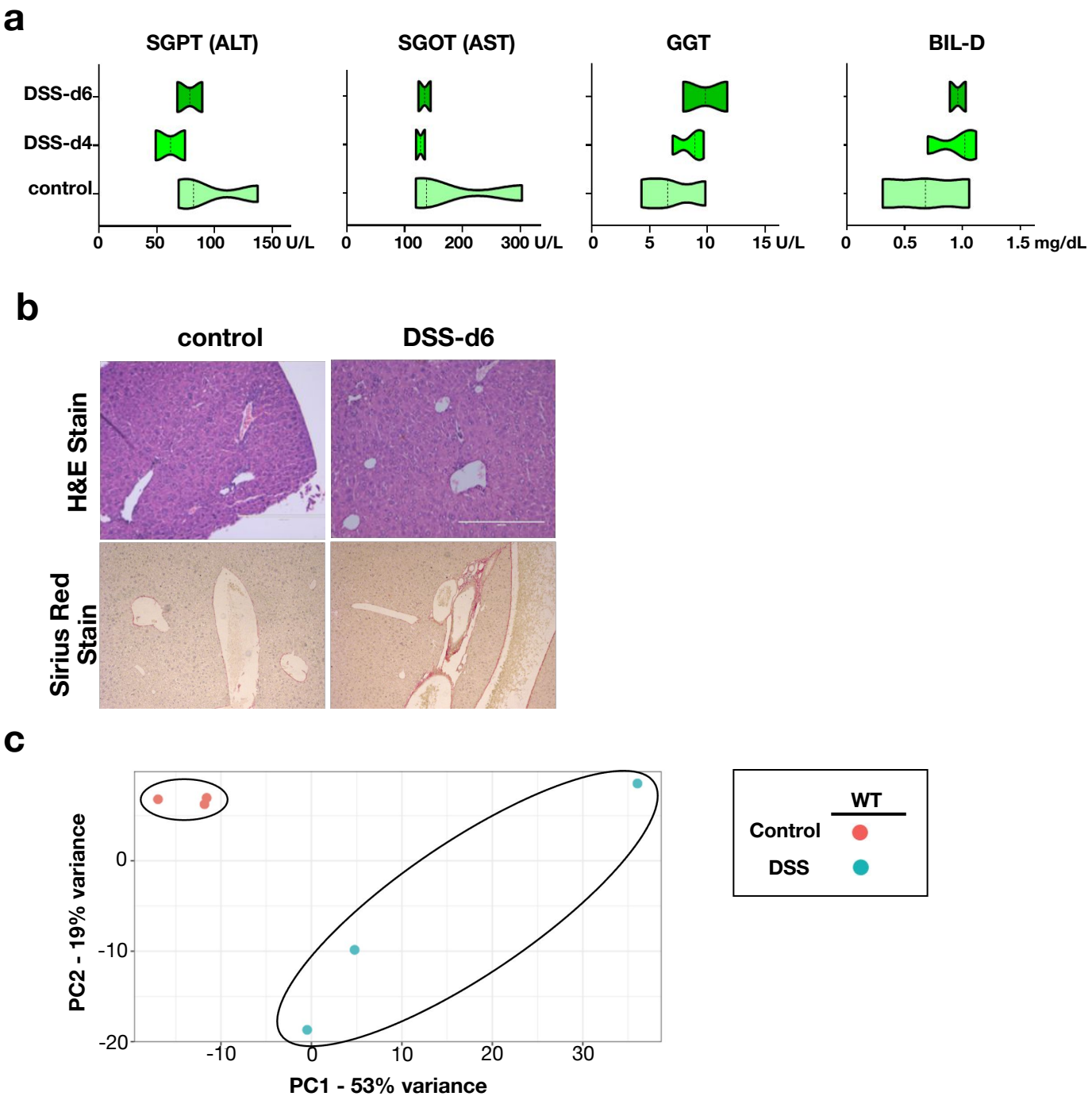

Figure S1: (a) Violin plot comparing the clinical parameter in serum of untreated and DSS treated wildtype mice (n=3) **(b)** Liver sections from untreated and DSS-treated wildtype mice were examined for histological features involving H&E staining [upper panel] and Sirius red staining [lower panel]. Data were obtained in 10X magnification and represent three experimental replicates; two fields per section and a total of three sections from each set were examined. **(c)** PCA plot illustrating the hepatic transcriptome, identified through global RNA-seq analyses, of untreated or DSS treated wildtype mice (n=3).

Supplementary Figure S1

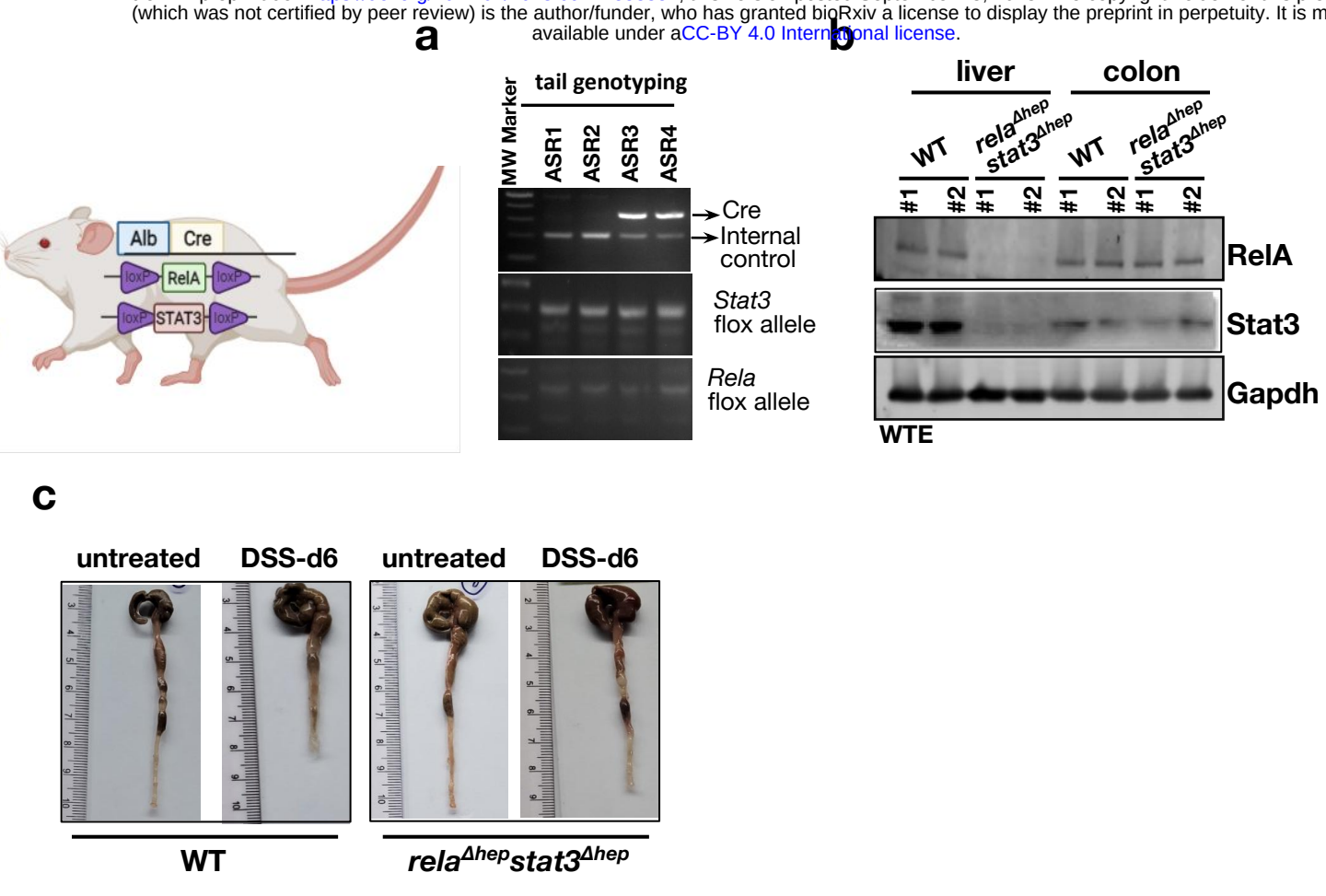

Figure S2: Characterization of mice strain by **(a)** genotyping and **(b)** western blotting. **(c)** Representative images of colon from untreated and DSS-treated wildtype and *rela*$^{\Delta hep}$*stat3*$^{\Delta hep}$ mice.

Figure S2

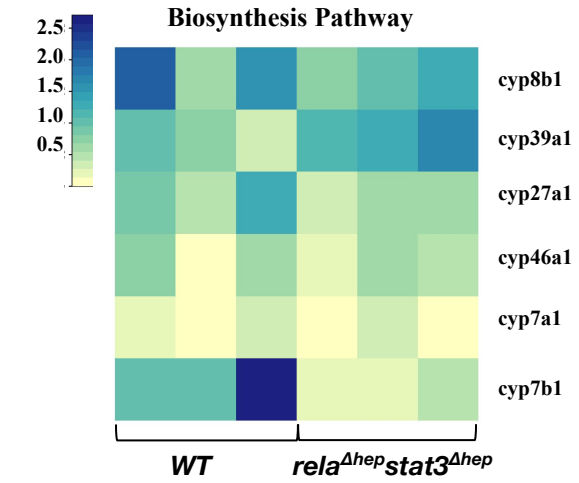

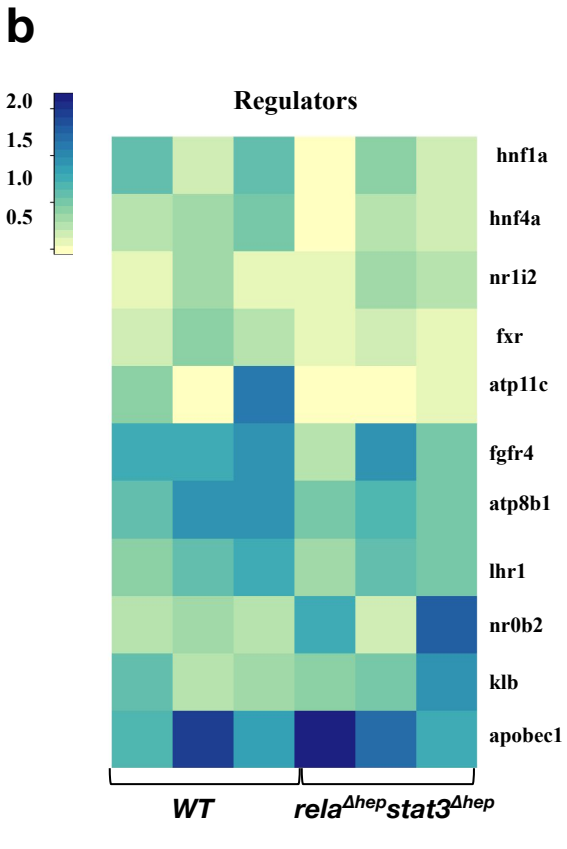

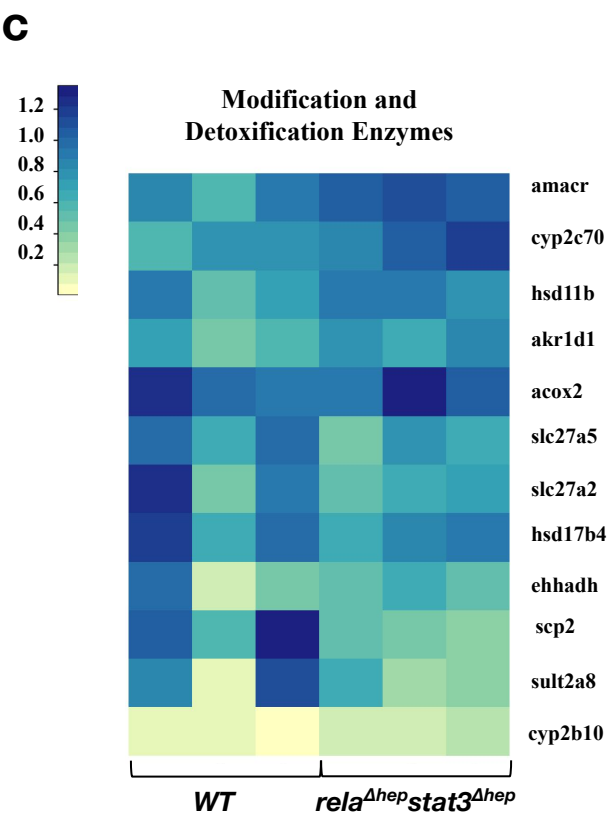

Figure S3: Heatmap represents relative transcript abundance of **(a)** biosynthesis pathway **(b)** regulators of bile acid metabolic pathways and **(c)** modification enzymes of bile acid metabolic pathway of indicated genotypes obtained from the RNA-seq experiment of three biological replicates.

Figure S3

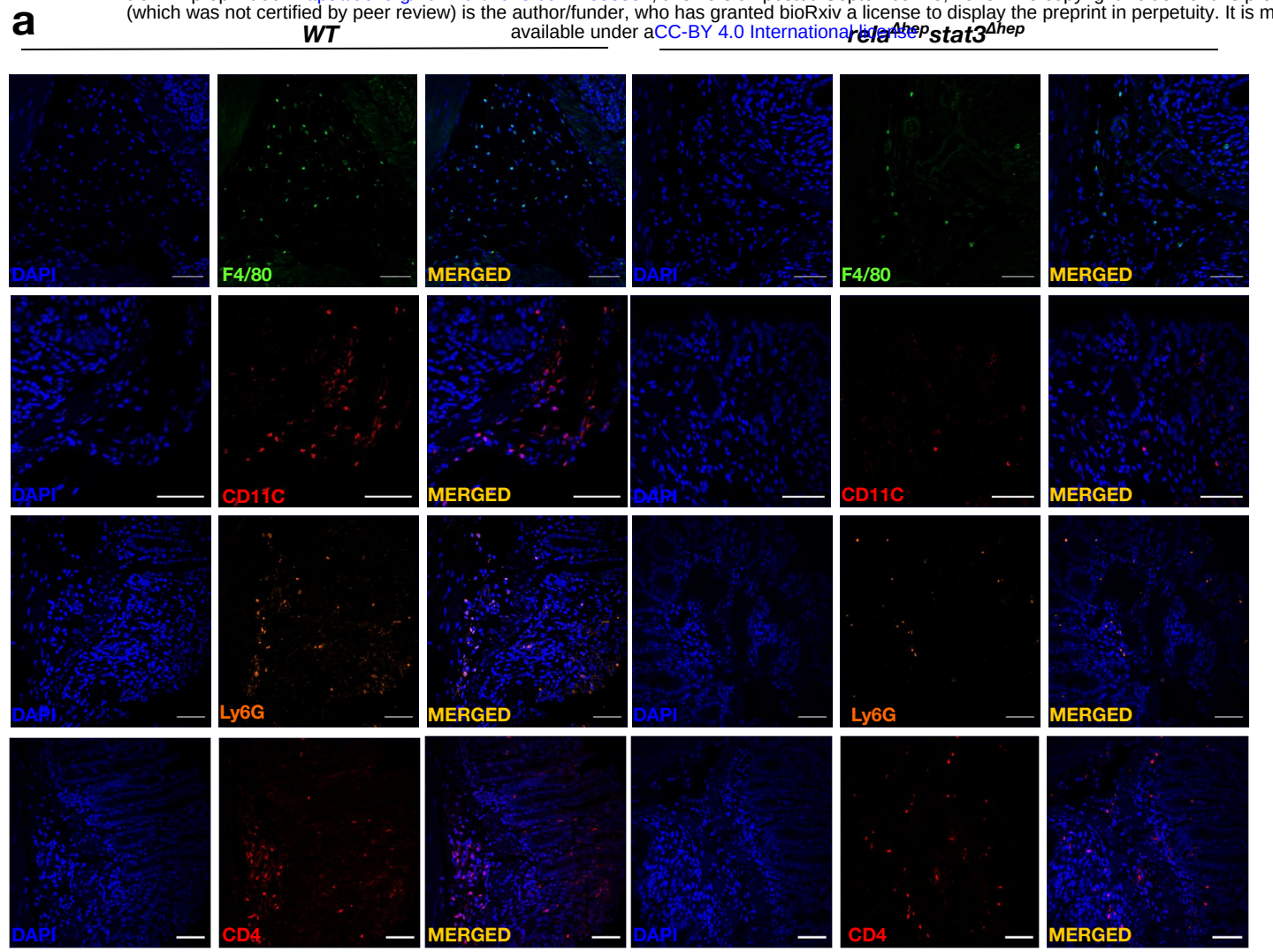

Figure S4: Representative images of colon tissue stained with indicated immune cell marker, DAPI and merged section in the DSS-treated wildtype and *rela*$^{\Delta hep}$*stat3*$^{\Delta hep}$ mice.

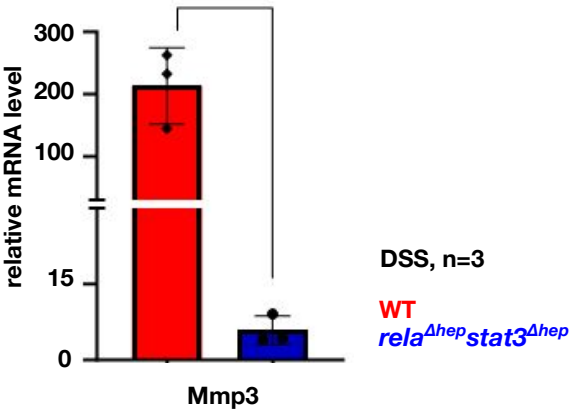

Figure S4

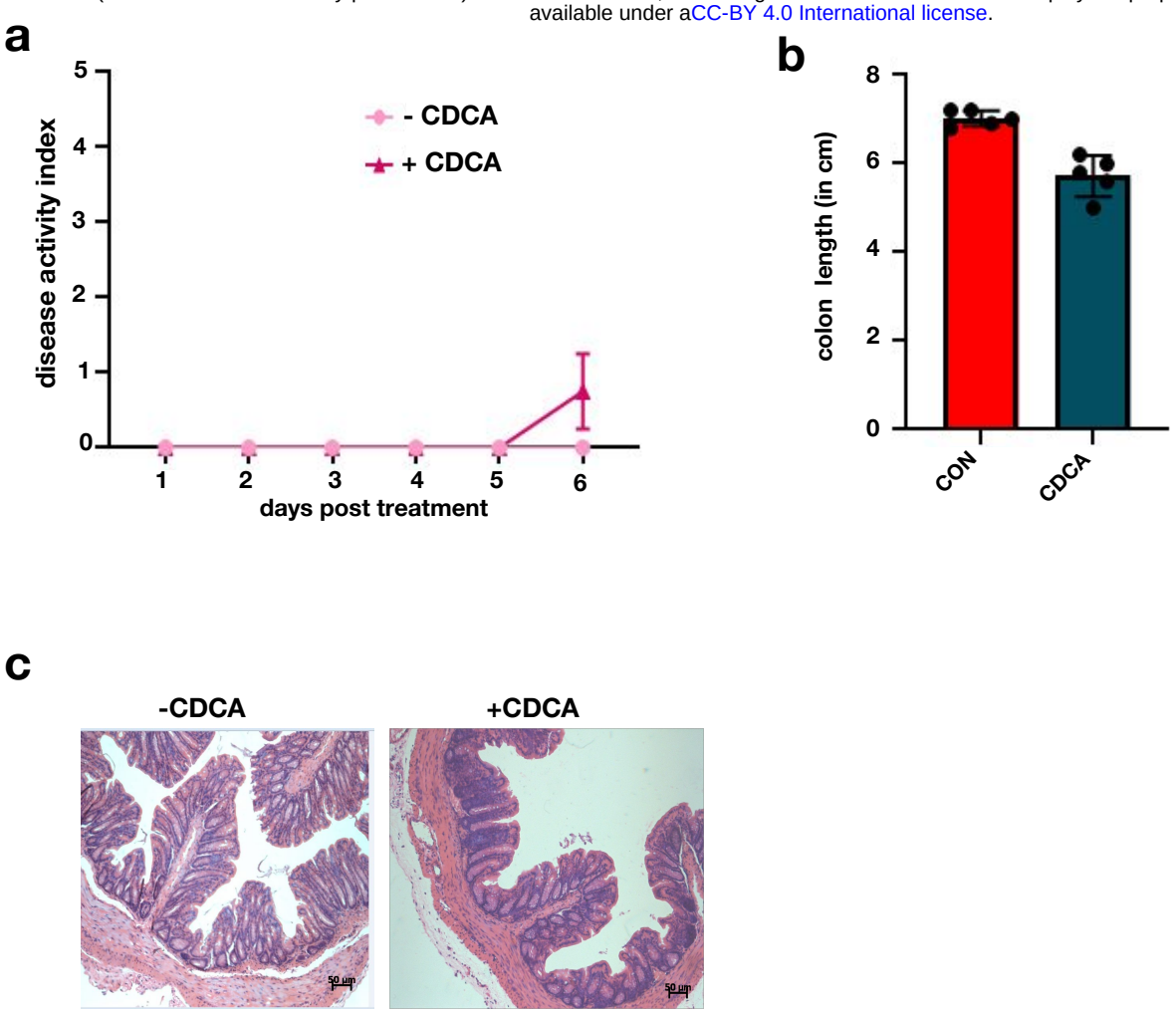

Figure S5: (a) Line plot charting the disease activity in a time course of *rela*$^{\Delta hep}$*stat3*$^{\Delta hep}$ mice subjected to daily supplementation of 10 mg/kg CDCA. Mice devoid of CDCA supplementation were treated with DMSO as controls. **(b)** Bar plot comparing the colon length of *rela*$^{\Delta hep}$*stat3*$^{\Delta hep}$ mice subjected to CDCA supplementation. **(c)** Colon sections from *rela*$^{\Delta hep}$*stat3*$^{\Delta hep}$ mice supplemented with CDCA were examined by H&E staining.

Figure S5

Table S1: List of antibodies

Antibody	Source	Identifier	RRID
PE rat anti-mouse Ly-6G	BD Biosciences	551461	AB_394208
FITC anti-mouse F4/80	BioLegend	157309	AB_2876535
PE anti-mouse CD11c	BioLegend	117308	AB_313777
PE anti-mouse CD4	BioLegend	100408	AB_312693
STAT3 mouse mAb	Thermo Fisher Scientific	MA1-13042	AB_10985240
RelA rabbit pAb	Santa Cruz Biotechnology	sc372	AB_632037
Phospho-Stat3 (Ser727) Rabbit mAb	Cell Signaling Technology	34911	AB_2737598
Phospho-Stat3 (Tyr705) Rabbit mAb	Cell Signaling Technology	9145	AB_2491009
Phospho-NF-κB p65 (Ser536) pAb	Cell Signaling Technology	3031	AB_330559
GAPDH rabbit mAb	Cell Signaling Technology	2118	AB_561053
β-Actin rabbit pAb	Cell Signaling Technology	4967	AB_330288
Goat anti-Rabbit IgG (H+L) Secondary Antibody Alexa Fluor Plus 555	Thermo Fisher Scientific	A32732	AB_2633281

Table S2: List of mice strain

Mice strain	Source	Identifier
C57BL/6 WT mice	available at the Small Animal Facility in NII	N/A
Alb_Cre rela$^{-/-}$ *stat3*$^{-/-}$ mice	gift from Dr. Lee Quinton (Boston University)	N/A
rela$^{fl/fl}$ stat3$^{fl/fl}$ mice	gift from Dr. Lee Quinton (Boston University)	N/A
Alb_Cre rela$^{-/-}$ mice	gift from Dr. Lee Quinton (Boston University)	N/A
rela$^{fl/fl}$ mice	gift from Dr. Lee Quinton (Boston University)	N/A
Alb_Cre stat3$^{-/-}$ mice	gift from Dr. Lee Quinton (Boston University)	N/A
stat3$^{fl/fl}$ mice	gift from Dr. Lee Quinton (Boston University)	N/A

Table S3: List of genotyping primers

Target gene	Sense strand	Antisense strand
Cre	5’-GGTGAACGTGCAAAACAGGCTC-3’	5’-AAAACAGGTAGTTATTCGGATCATCAGC-3’
Tcrd (Internal control)	5’-CAAATGTTGCTTGTCTGGTG-3’	5’-GTCAGTCGAGTGCACAGTTT-3’
Floxed Stat3	5’-CCTGAAGACCAAGTTCATCTGTGTTGAC-3’	5’-CACACAAGCCATCAAACTCTGGTCTCC-3’
Floxed Rela	5’-GAGCGCATGCCTAGCACCAG-3’	5’-GTGCACTGCATGCGTGCAG-3’

Table S4: List of primers

Target gene	Sense strand	Antisense strand
Tight junction protein 1 (tjp1)	5'-GCTTTAGCGAACAGAAGGAGC-3'	5'-TTCATTTTTCCGAGACTTCACCA-3'
Occludin (ocln)	5'-TGAAAGTCCACCTCCTTACAGA-3'	5'-CCGGATAAAAAGAGTACGCTGG-3'
Mucin 2 (muc2)	5'-AGGGCTCGGAACTCCAGAAA-3'	5'-CCAGGGAATCGGTAGACATCG-3'
Trefoil factor 3 (tff3)	5'-TTGCTGGGTCCTCTGGGATAG-3'	5'-TACACTGCTCCGATGTGACAG-3'
Interleukin-1β (il1β)	5'-CATCCCATGAGTCACAGAGGATG-3'	5'-ACCTTCCAGGATGAGGACATGAG-3'
Tumor necrosis factor α (tnfα)	5'-CTGAACTTCGGGGTGATCGG-3'	5'-GGCTTGTCACTCGAATTTTGAGA-5'
Interleukin-6 (il6)	5'-CCCCAATTTCCAATGCTCTCC-3'	5'-GGATGGTGTTGGTCCTTAGCC-3'
Metallomatrix protease 3 (mmp3)	5'-GGCCTGGAACAGTCTTGGC-3'	5'-TGTCCATCGTTCATCATCGTCA-3'
gapdh	5'-AGGTCGGTGTGAACGGATT-3'	5'-AATCTCCACTTTGCCACTGC-3'
cyp7a1	5'-GCTGTGGTAGTGAGCTGTTG-3'	5'-GTTGTCCAAAGGAGGTTCACC-3'
cyp8b1	5'-CCTCTGGACAAGGGTTTTGTG-3'	5'-GCACCGTGAAGACATCCCC-3'
cyp27a1	5'-AGGGCAAGTACCCAATAAGAGA-3'	5'-TCGTTTAAGGCATCCGTGTAGA-3'
cyp7b1	5'-TCCTGGCTGAACTCTTCTGC-3'	5'-CCAGACCATATTGGCCCGTA-3'

Table S5: List of reagents

Reagent	Source	Identifier
Chemicals and Peptides		
DSS (40,000 MW)	Sigma-Aldrich	42867
FITC-Dextran (MW 3000 - 5000)	Sigma-Aldrich	60842-46-8
Immobilon Forte Western HRP Substrate	Millipore	WBLUF0500
Amersham™ Hybond® P Western blotting membranes, PVDF	Merck	10600023
1.0 mm Zirconia/Silica	BioSpec Product	11079110z
Chenodexycholic acid	Sigma-Aldrich	474-25-9
DAPI	Sigma-Aldrich	D9542
PowerUp SYBR	Thermo Fisher Scientific	A25742
Fluorosheild	Sigma-Aldrich	F6182
Commercial Kits		
NucleoSpin RNA	Macherey-Nagel	74106
Primescript 1st strand cDNA synthesis kit	Takara Bio	6110A

Table S6: Control patient demography

Sample code	Sample type	Age (years)	Gender (1=Male)	BMI
01-C-F	Control	50	2	24.6
02-C-F	Control	35	1	21.8
03-C-F	Control	50	1	16.9
04-C-F	Control	27	2	17.7
05-C-F	Control	42	2	23.4
06-C-F	Control	36	1	25
07-C-F	Control	54	1	21.3
08-C-F	Control	52	2	23.3
10-C-F	Control	19	1	21.17
12-C-F	Control	30	1	17.8
13-C-F	Control	28	1	21.3
14-C-F	Control	59	2	20.2
16-C-F	Control	32	1	23.5

Table S7: UC patient demography

Sample code	Sample type	Age (years)	Gender (1=Male)	BMI
01-A-F	UC	50	2	25
02-A-F	UC	44	1	24
03-A-F	UC	29	1	16
04-A-F	UC	25	1	15
05-A-F	UC	32	1	18
06-A-F	UC	50	2	23
07-A-F	UC	24	1	17
08-A-F	UC	50	1	26
09-A-F	UC	27	2	22
10-A-F	UC	35	1	20
11-A-F	UC	22	2	18
12-A-F	UC	25	2	23
13-A-F	UC	30	1	29
14-A-F	UC	26	1	17
15-A-F	UC	25	2	17
17-A-F	UC	24	2	29
18-A-F	UC	26	1	21
19-A-F	UC	45	2	21
20-A-F	UC	23	1	18
21-A-F	UC	24	2	17
22-A-F	UC	26	1	17
23-A-F	UC	50	2	37
24-A-F	UC	43	1	25
25-A-F	UC	30	2	23
26-A-F	UC	31	1	16
27-A-F	UC	32	1	19
28-A-F	UC	26	1	23

Figure 1 - source data 1 : List of all the GO enrichment terms along with their pValues that are differentially regulated in the DSS treated wild type animals in comparison to untreated wild type animals. This data has been utilized to build the pathway enrichment map in Figure 1A.

Figure 1 - source data 2 : Values of the quantified blot that was utilized to build the bar plot in figure 1E. The p values used to compare the groups have also been added.

Figure 1 - source data 3 : Unedited and uncropped blot that are represented in figure 1D.

Figure 2 - source data 1 : Values for the DAI utilized for the line graph in figure 2A. Along with the p value used to compare the groups.

Figure 2 - source data 2 : Values for the colon length utilized for the bar graph in figure 2B. Along with the p value used to compare the groups.

Figure 2 - source data 3 : Values of the leaked FITC-dextran measure from the sera utilized to construct the bar plot in figure 2D. Along with the p value used to compare the groups.

Figure 2 - source data 4 : Values for the calculated fold change for the transcript levels of the respective genes utilized for the bar graph in figure 2E. Along with the p value used to compare the groups.

Figure 3 - source data 1 : List of all the GO enrichment terms along with their pValues that are differentially regulated in the DSS treated wild type cluster as well as the knockout cluster. This data has been utilized to build the pathway enrichment map in Figure 3B.

Figure 3 - source data 2 : Metabolite quantification data for patient biopsy for the IBD and Non-IBD group utilized for the bar plot in figure 3C and p value calculation that has been used to compare across groups.

Figure 3 - source data 3 : Values for the calculated fold change for the transcript levels of the respective genes utilized for the bar graph in figure 3E. Along with the p value used to compare the groups.

Figure 4 - source data 1 : Metabolite quantification data for liver tissue and colon tissue utilized for the bar plot in figure 4A and figure 4B. Along with the p value calculation that has been used to compare across groups.

Figure 4 - source data 2 : Values of quantification of the confocal microscopy for different fields and the p value used to compare across groups plotted as dot plot in figure 4C.

Figure 4 - source data 3 : Values for the calculated fold change for the transcript levels of the respective genes utilized for the bar graph in figure 4D. Along with the p value used to compare the groups.

Figure 5 - source data 1 : Values of measured disease activity index and colon length and respective p values used to compare across groups, plotted in figure 5A and 5B.

Figure 5 - source data 2 : Values for the calculated fold change for the transcript levels of the respective genes utilized for the bar graph in figure 5D and 5E. Along with the p value used to compare the groups.

Supplementary - source data 1: value used to generate the violin plot in supplementary figure S1a.

Supplementary - source data 2: uncropped and unedited gels for supplementary figure S2a.

Supplementary - source data 3: uncropped and unedited blots for supplementary figure S2b.